Fluvial response to horizontal shortening: a study in the Southern Alps of New Zealand

Frédéric Herman, Jean Braun

Fluvial response to horizontal shortening and glaciations: A study in the Southern Alps of New Zealand

Frédéric Herman[1,2] and Jean Braun[1,3]

Received 8 October 2004; revised 22 July 2005; accepted 26 September 2005; published 11 February 2006.

[1] It has been postulated that a steady state between erosional and tectonic processes may develop in continental collision. However, it is not clear whether steady state conditions can be reached for all components of the landscape. Here we show, using landscape evolution models and field evidence, that a true geomorphic steady state may never be reached in the Southern Alps of New Zealand. The strong asymmetries in tectonic uplift and tectonic advection and the onset of glaciations constantly interact to prevent the landscape from reaching a topographic steady state. Evidence suggests that the first-order geomorphology on the western side of the Southern Alps is controlled by orographic precipitation combined with extreme rates of tectonic uplift, whereas the development of deep glacial valleys on the eastern side is initiated by differential uplift along large faults. We also develop a first-order equation, governing the dynamics of the Main Divide, to show that both tectonic advection and fluvial erosion efficiency control the position and the height of the main drainage divide. Using a two-dimensional landscape evolution model, we demonstrate that the transition from glacial to fluvial conditions at the end of the last glaciation led to substantial modifications of the landscape: While the main trunk channels get slowly uplifted, ridges are leveled down, causing the relief to decrease. Hillslopes appear to be affected by fluvial processes which seem to be driven by incision of river tributaries. This reduction of relief will probably never reach a steady state since warmer interglacial periods are substantially shorter than glacial periods.

Citation: Herman, F., and J. Braun (2006), Fluvial response to horizontal shortening and glaciations: A study in the Southern Alps of New Zealand, *J. Geophys. Res.*, *111*, F01008, doi:10.1029/2004JF000248.

1. Introduction

[2] In recent years much effort has been devoted to understanding the interactions between climate, tectonics and surface processes and the role they play during mountain building episodes [e.g., *Raymo and Ruddiman*, 1992; *Avouac and Burov*, 1996; *Beaumont et al.*, 2001; *Reiners et al.*, 2003]. The rise of large mountain ranges leads to local and global climate changes including increased precipitation which can enhance erosion. This potentially leads to a feedback mechanism toward more focused and higher rates of tectonic uplift [*Molnar and England*, 1990; *Beaumont et al.*, 2004]. The Earth's surface can therefore be regarded as one of the locations where endogenic processes (i.e., tectonics) and exogenic processes (i.e., mainly erosion and climate) work hand in hand to produce or reduce relief. Understanding and quantifying the processes that affect topography, its organization as well as its dynamics is crucial to understanding how external processes and erosion interact with each other and, potentially, balance to reach equilibrium.

[3] The rate at which relief production or reduction responds to changes in external (climatic) conditions has recently become a matter of active debate [e.g., *Molnar and England*, 1990; *Brozovic et al.*, 1997; *Small and Anderson*, 1998; *Whipple et al.*, 1999; *Brocklehurst and Whipple*, 2002]. In particular, *Molnar and England* [1990] argued that a transition to cooler climatic conditions may induce an increase in mean erosion rate and, ultimately, be responsible for an apparent enhancement in rock uplift. These authors also stated that an increase in erosion rates will lead to relief production and isostatically driven uplift of mountain peaks. *Whipple et al.* [1999] questioned the former assertion and showed that climate change to colder conditions may in fact lead to relief reduction in both glaciated and nonglaciated landscapes (i.e., an increase in fluvial erosivity and/or the transition from fluvial to glacial erosion will reduce relief rather than increase it). It is interesting to note, however, that some of the constraints on this debate are obtained from field observations in active orogens characterized by postglacial landscapes where fluvial erosion is relatively far from steady state conditions and could therefore be anomalously efficient at destabilizing the landscape [*Pratt-*

[1]Research School of Earth Sciences, Australian National University, Canberra, ACT, Australia.
[2]Now at California Institute of Technology, Pasadena, California, USA.
[3]Now at Géosciences Rennes, Université de Rennes 1, Rennes, France.

0148-0227/06/2004JF000248

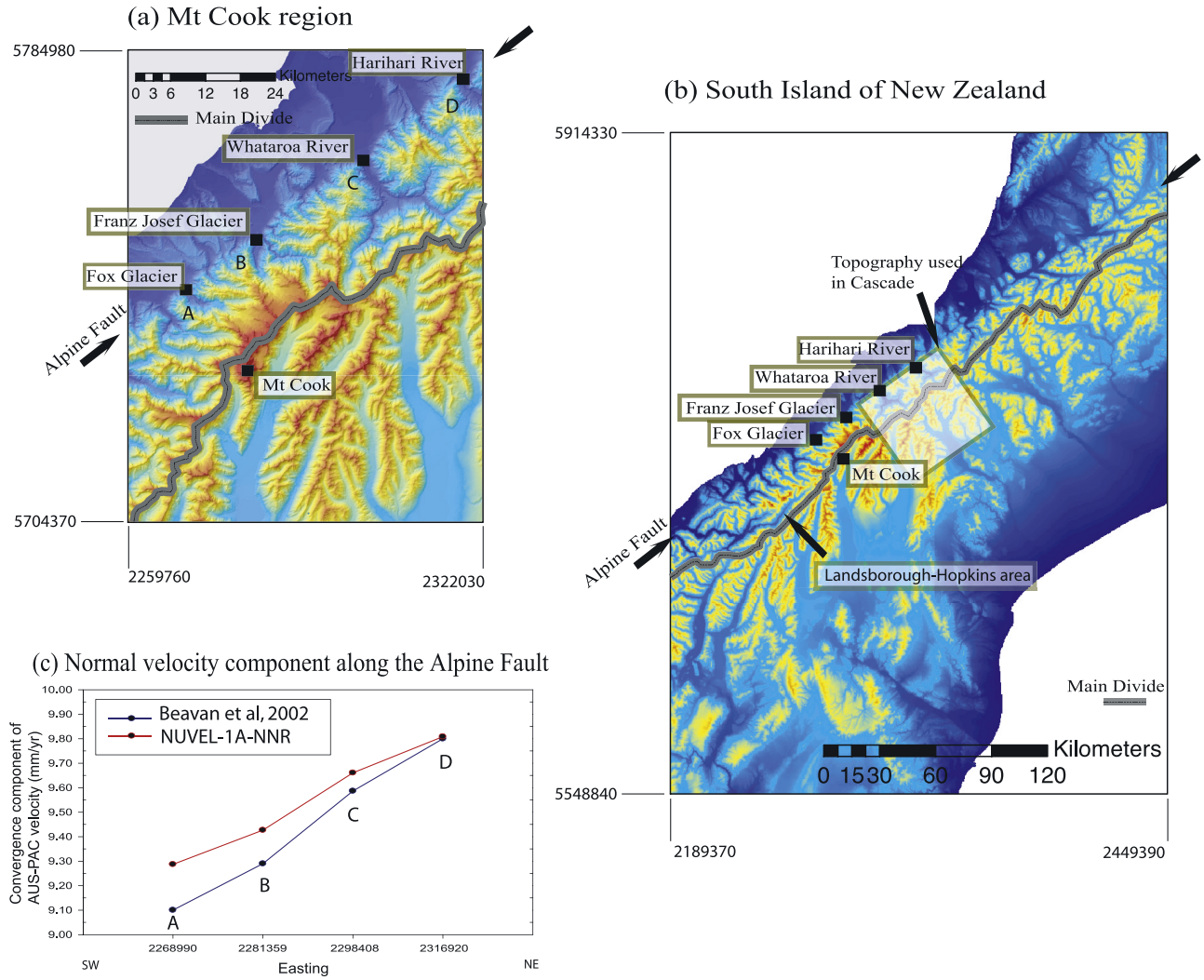

Figure 1. Location of the main drainage divide (a) in the central part of South Island, near Mount Cook, and (b) at the scale of South Island (these images are extracted from a 50 m digital elevation model (Terralink)). The position of the divide with regard to the Alpine Fault is characterized by segmentation of 10–30 km length segments subparallel to the fault. In the Whataroa River region, the divide appears to be at lower altitude and farther away from the Alpine Fault than in the Franz Josef Glacier area. To the south of Mount Cook, the divide position is gradually farther away from the fault (Landsborough-Hopkins area) and finally, closer in the most southern part. New Zealand map grid coordinate system is adopted here, as well as for the other figures. (c) Variation of the convergent component of relative Pacific-Australian plate velocity along the central section of the Alpine Fault. Euler velocities at four locations along the Alpine Fault (A to D; see Figure 1a) are inferred from *Beavan et al.* [2002] and NUVEL-1A.

Sitaula et al., 2004]. For example, *Hovius et al.* [1997] highlighted the importance of landslides resulting from rapid river incision in previously glaciated valleys which may have become the most efficient process reshaping the landform during postglacial periods. Therefore quantitative estimates on landform evolution during the glacial-interglacial transition should improve our current understanding of the relief development in active mountain belts responding to climate change and tectonic forcing.

[4] Numerical models of continental collision [*Beaumont et al.*, 1996a; *Batt and Braun*, 1997, 1999; *Koons et al.*, 2002; *Willett*, 1999] have shown how concentrated erosional activity may significantly affect the development of an orogen. The link between drainage reorganization and tectonic processes is often highlighted in regions where erosion and deformation are focused [*Zeitler et al.*, 2001; *Beaumont et al.*, 2001; *Wobus et al.*, 2003]. Most orogens show drainage patterns that are distinctly organized on either side of the main drainage divide. Examples include the Andes, Taiwan, and the Southern Alps of New Zealand, where the divide separates regions of contrasting landforms and variable exhumation rate. Divide migration by tectonic horizontal advection has therefore the potential to significantly perturb drainage systems and, in turn, affect the complex patterns of rock uplift and exhumation in an active orogen. Although there is ample field evidence of rapid

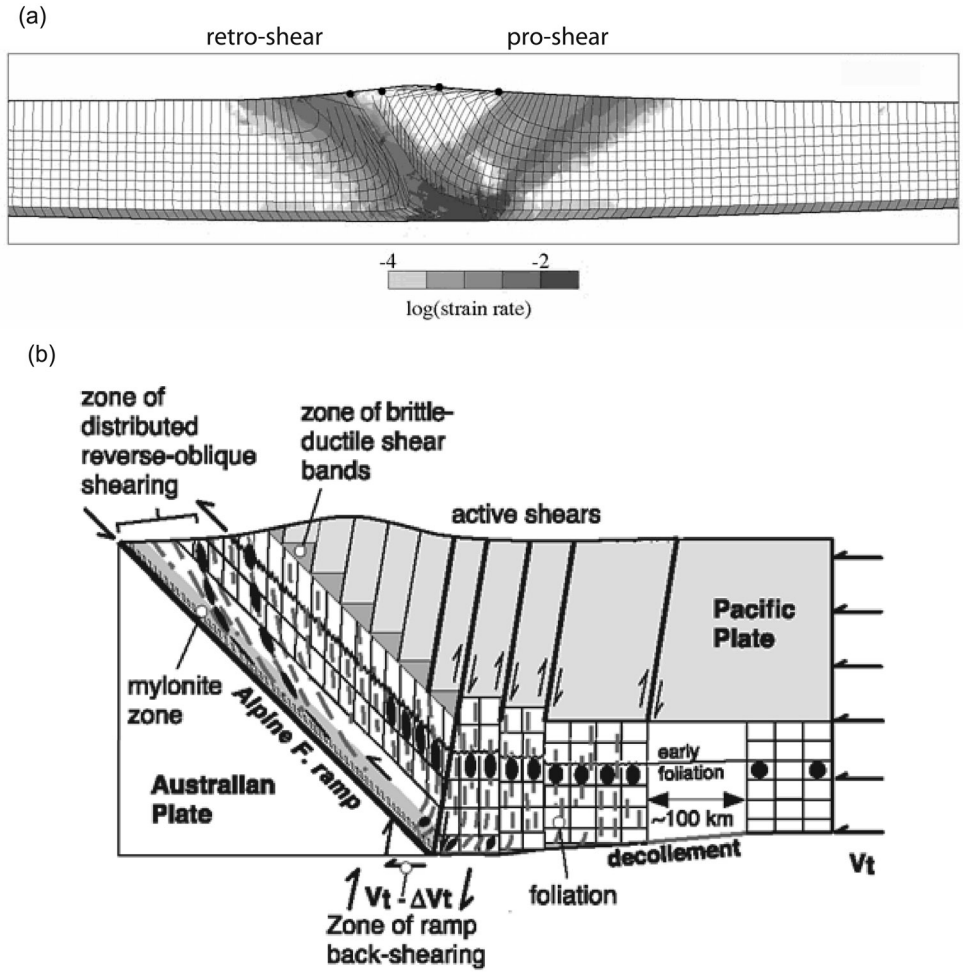

Figure 2. (a) Results from a numerical model [*Batt*, 1997] in which collision is accommodated by mantle subduction and upthrusting of the Pacific plate onto the Australian plate. (b) Idealized cross-sectional model of the orogen [*Little and Holcombe*, 2002].

divide migration in active mountain belts [*Schlunegger and Hinderer*, 2001; *Craw et al.*, 2004], the nature of the mechanism(s) by which it takes place remains unclear. Indeed, most models of landscape evolution commonly assume that bedrock incision and hillslope erosion are the most efficient erosional processes in high-relief terrains. However, since drainage area vanishes near the top of a ridge, bedrock incision is very slow and hillslope processes must dominate. Alternatively, it may be that most episodes of drainage migration take place during glacial times when ice flows over and, potentially, erodes local topographic divides.

[5] In this paper we address two issues and ultimately discuss their potential consequences: (1) How does relief evolve during the transition from glacial to postglacial conditions? (2) What are the processes controlling the position of the main drainage divide? In an attempt to provide answers to these questions, we focus on the Southern Alps of New Zealand, an orogen formed by rapid convergence between the Pacific and Australian plates, which is also known to have been strongly glaciated [e.g., *Willett*, 1950; *Porter*, 1975; *Soons*, 1979; *Adams*, 1980; *Whitehouse*, 1987; *Tomkin*, 2000; *Barrows et al.*, 2000]. Extensive data sets have been collected [e.g., *Kamp and Tippett*, 1993; *Koons*, 1994; *Davey et al.*, 1995; *Batt*, 1997; *Walcott*, 1998; F. Herman et al., Tectonomorphic scenarios in the Southern Alps of New Zealand, submitted to *Journal of Geophysical Research*, 2005, hereinafter referred to as Herman et al., submitted manuscript, 2005] that provide good constraints on the tectonic setting of the collision and enable us to focus on the reshaping of the landscape during the glacial-interglacial transition. Furthermore, a closer look at the geometry of the drainage divide demonstrates that it is a segmented feature, not a linear one. Figure 1 shows the location of the main drainage divide in the Southern Alps of New Zealand. The divide is subparallel to the Alpine Fault, the oblique-reverse fault that accommodates convergence in this orogen, but its exact geometry is segmented at a wavelength of 10 to 30 km. In the light of this simple observation and recent studies implying divide migration [*Willett et al.*, 2001; *Craw et al.*, 2004], we explore here how the dynamics of the divide could be related to horizontal tectonic advection and/or erosional processes.

[6] We first describe the geological and geomorphological setting of the area. We review the existing evidence on the nature of the various processes that control the large-

scale evolution of the landscape in the Southern Alps. We then investigate the extent to which bedrock incision influences the stability and position of the main drainage divide by solving a simple one-dimensional (1-D) equation, which expresses the balance between erosion, tectonic uplift and horizontal advection. We then use a 2-D landscape evolution model to estimate which parts of the present-day surface topography are most affected by the transition from a glacial- to fluvial-dominated erosion. Finally, we discuss how horizontal advection of landform, divide migration and climate oscillations may control the long-term organization of the landscape.

2. Tectonic Setting and Collision Geometry in the Southern Alps of New Zealand

[7] The Southern Alps of New Zealand are the result of the ongoing oblique continental collision between the Pacific and Australian Plates [*Wellman*, 1979]. The present-day relative plate motion has a large strike-slip component (~33–40 mm/yr) compared to its normal component (~8–10 mm/yr). Most of the oblique deformation is thought to be taken up by a single structure called the Alpine Fault (Figures 1 and 2) which also accommodates ~75% of the normal component. The remaining part of the convergence between the two plates is accommodated by distributed shortening in the Southern Alps [*Norris et al.*, 1990; *Walcott*, 1998; *Little and Holcombe*, 2002]. It is commonly assumed that the incoming Pacific plate delaminates [*Wellman*, 1979], with material from above 25 km depth brought to the surface along the Alpine Fault, while lower crustal material is either added to an assumed orogenic root or subducted with the Pacific lithospheric mantle (Figure 2). According to *Koons* [1994], *Beaumont et al.* [1996b], and *Batt and Braun* [1999], this orogen behaves like a doubly sided critical taper bounded by two oppositely dipping structures: the retroshears and proshears. The former, located on the "stable" continent side and accumulating large deformation, is commonly associated with the Alpine Fault; the later, being the locus of instantaneous deformation, leads to the formation of an array of structures antithetic to the Alpine Fault that are progressively advected into the orogen by movement along the Alpine Fault. This scenario is supported by geological and geophysical evidence [*Allis*, 1981, 1986; *Craw et al.*, 1994; *Stern*, 1995; *Davey et al.*, 1995; *Beavan et al.*, 1999]. The orogen is thought to have reached a flux steady state [*Willett and Brandon*, 2002] a few millions years after the present-day collision initiated some 6 Ma ago [*Batt*, 1997]. The rapid convergence between the two plates and the relatively narrow region of documented uplift, erosion and thus exhumation along the western slopes of the mountain belt result in a relatively well constrained exhumation rate of ~8–10 mm/yr, or 800–1000 m of rocks denuded over the last 100 kyr.

[8] Rock uplift and exhumation are strongly asymmetric [*Kamp and Tippett*, 1993] and controlled in part by the equally strong asymmetry in precipitation [*Griffiths and McSaveney*, 1983] on either sides of the main drainage divide: while up to 12 m/yr of precipitation falls on the western flank of the orogen, the eastern slopes remain relatively dry with a mean annual precipitation of only 1 m/yr.

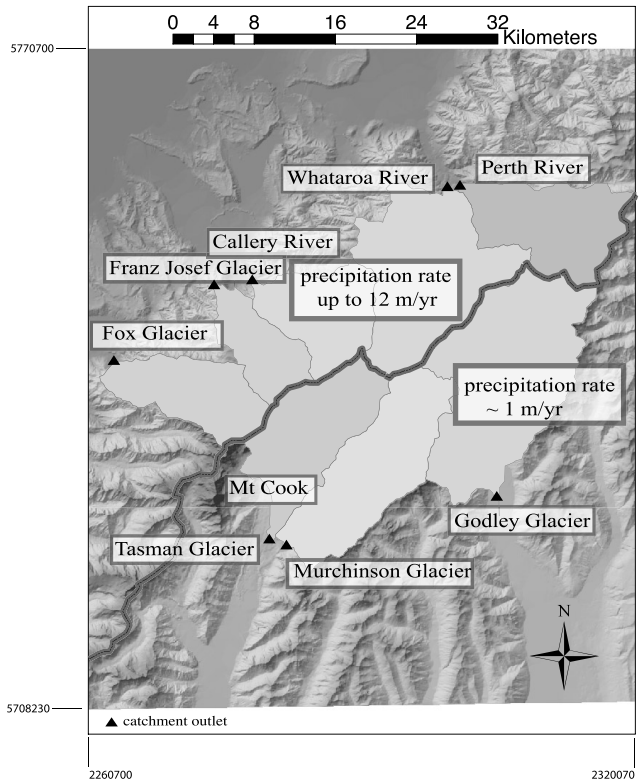

Figure 3. Geometry of drainage basins in the central part of the Southern Alps. Triangles indicate the positions of catchment outlets. On the western side of the divide, the basins are perpendicular to the divide, whereas on the eastern side they are parallel to it. The Whataroa and Perth basins are characterized by a transitional geometry.

[9] Contemporary GPS measurements show variation in the convergent component of relative Pacific-Australian plate velocities along the central section of the Alpine Fault. Calculated relative velocities inferred from *Beavan et al.* [2002] and NUVEL-1A are shown in Figure 1c. This illustrates that the convergence rate is increasing from southwest to northeast along the Alpine Fault. Furthermore, surface strain rate estimates derived from GPS velocities [*Beavan et al.*, 2002] indicate that shortening in the Southern Alps is accommodated in the vicinity of the Alpine Fault (the retroshear) and on the other side of the orogen, that is, where the doubly vergent critical taper model (Figure 2) predicts shortening by reverse movement along the proshear.

3. Erosional and Structural Control on the Geomorphology of the Southern Alps

[10] The geometry of drainage basins in the central part of the collision (Figure 3) shows clear variations in size, shape and azimuth on either side of the Main Divide. On the eastern side, the catchments are large and subparallel to the divide. On the western side, most of the basins are smaller and subperpendicular to the divide, with the exception of

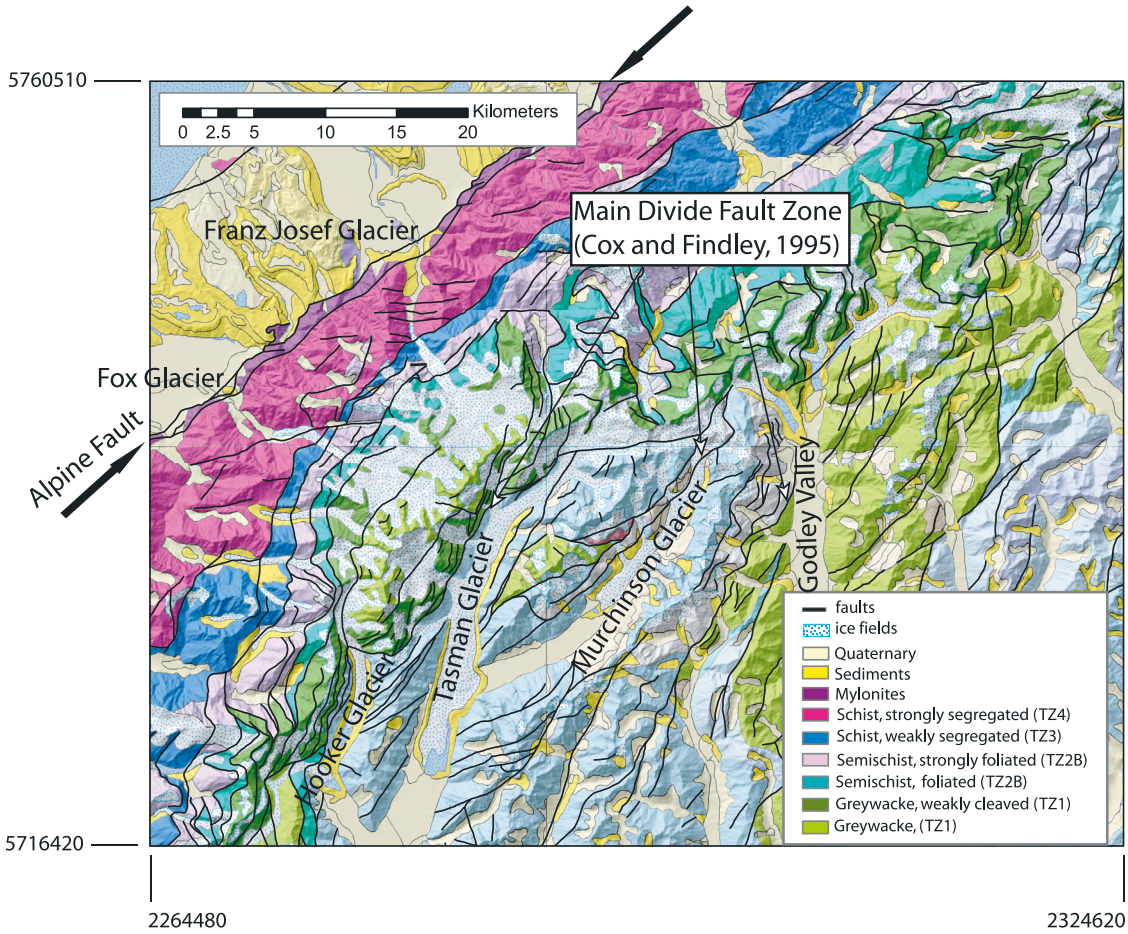

Figure 4. Simplified geological map of the Southern Alps of New Zealand (S. Cox, Institute of Geological and Nuclear Sciences (IGNS), personal communication, 2003) superimposed on shaded relief map. Note the strong structural control on the large glaciated valleys on the eastern side of the divide.

the Whataroa basin which is much larger and seems to have a more complex geometry.

[11] The extreme precipitation rate (up to 12 m/yr) and steep topographic gradient on the western side of the orogen easily explain why the drainage basins are narrow and subperpendicular to the divide. On the eastern side, the basins are elongated in a direction that is not perpendicular to the direction of maximum slope, indicating that the large-scale features of the landform are not controlled by a simple drainage organization along a gently dipping regional slope. It cannot be argued that the orientation of the drainage basins on the eastern side of the orogen, and the orientation of the large glacial valleys they host, is controlled by the strike-slip component of deformation between the two colliding plates, as most of the strike-slip deformation is accommodated by oblique slip along the Alpine Fault [*Beavan et al.*, 1999] which is completely disconnected from the drainage patterns on the eastern side of the orogen by the drainage divide.

[12] *Koons* [1994] described the Southern Alps as a two-sided orogen in which, on the eastern side of the divide, the landscape is mainly structurally controlled, that is, by movement along reverse, west dipping faults (Figures 2b and 4 [*Cox and Findley*, 1995; *Little and Holcombe*, 2002]). Along the western flank, landforms appear to be mainly controlled by precipitation-induced erosion. *Koons* [1994], *Willett et al.* [2001], and more recently, *Craw et al.* [2004] suggested that eastward draining catchments, such as in the Landsborough-Hopkins area, could be horizontally advected from drier regions east of the divide to regions of intense rainfall on the western side of the divide, and captured by westward draining rivers. *Craw et al.* [2004] also suggested that these captures may occur during short-lived, discrete events, causing the divide to migrate in a direction opposite to the direction of convergence.

[13] Little field evidence is available to conclusively determine which of the faults bounding the glacial valleys of the eastern slopes (Figure 4) are currently active or when they were active in the past [*Cox and Findley*, 1995]. Figure 4 shows a simplified geological map of the area on which the location of the major faults have been superimposed. The distinction between active and inactive faults remains, however, quite speculative because fault movement is difficult to document in a region characterized by a very homogeneous lithology (the Torlesse Greywacke and its metamorphosed equivalent, the Otago Schist) and no thermochronological estimate of fault activity is available to date. It is clear, however, that several of the large glacial

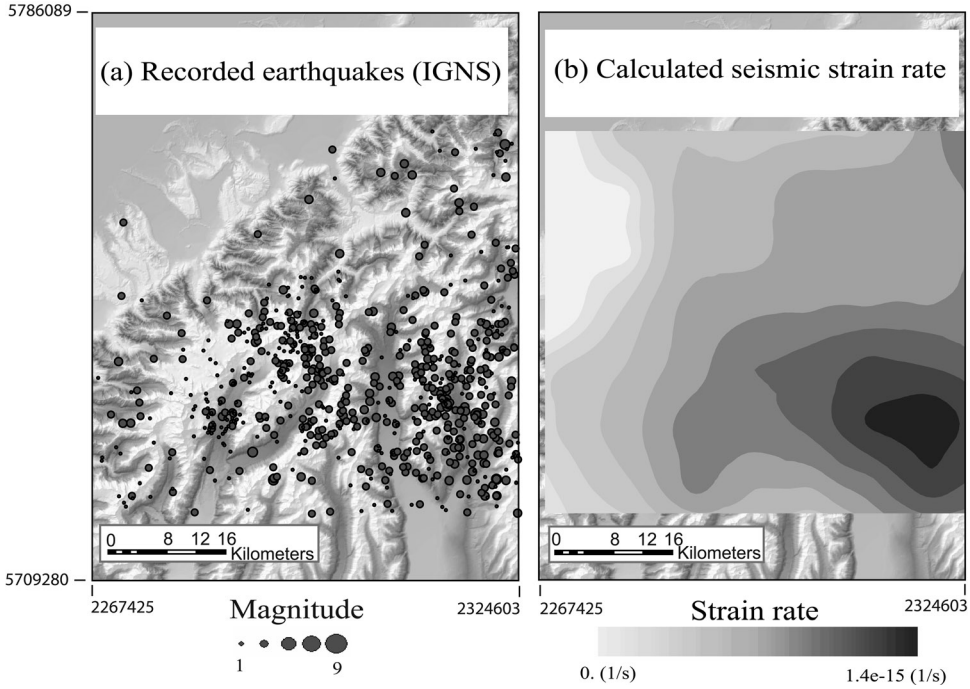

Figure 5. (a) Location of earthquakes observed during the last 50 years (from IGNS database). Magnitude varies from 3 to 6. Most earthquakes are situated in the upper crust, top 10 km. (b) Estimate of the seismic strain rate derived from earthquake magnitude data. The strain rate is maximum on the eastern side of the divide and decreases toward the divide.

valleys are bounded by faults that were active during the current Alpine orogeny [*Cox and Findley*, 1995]. These faults may correspond to the array of proshears (Figure 2) as predicted by the doubly vergent critical taper model [*Willett et al.*, 1993; *Batt and Braun*, 1999].

[14] Current fault movement (brittle deformation) can be estimated from the distribution of crustal seismicity. A large number of earthquakes have been recorded over the last 50 years in the Southern Alps and are shown in Figure 5a. For each earthquake, one can estimate the seismic strain rate and potentially the broad-scale distribution of current brittle deformation in the Southern Alps. To extract strain rate estimates from the earthquake database, we adopt the following procedure [*Gesto*, 2003]. We first bin all the earthquakes in 5 × 5 km cells. In each cell, we determine a best fit magnitude-frequency (M-N) relationship of the form [*Gutenberg and Richter*, 1944]

$$\log N = a - bM \tag{1}$$

Earthquake magnitude, M, can be related to the amplitude of the moment release, M_0, by the following empirical relationship [*Brune*, 1968]:

$$M_0 = 10^{M+12.2} \tag{2}$$

A seismic strain estimate can be derived from the amplitude of the moment release [*Kostrov*, 1974]:

$$\epsilon = \frac{M_0}{2\mu\Delta V} \tag{3}$$

where μ is the elastic shear modulus and ΔV the characteristic volume affected by the earthquake (for each cell: surface area × mean earthquake depth). Seismic strain rate, $\dot{\epsilon}$, within each cell can in turn be estimated by integrating the magnitude distribution up to an assumed maximum value, $M_{\max}$, and divide the resulting strain estimate by the observation timescale, Δt:

$$\dot{\epsilon} = \frac{b10^{a+12.2}\left(10^{(1-b)M_{\max}} - 1\right)}{\triangle t(2\mu\triangle V)(1-b)} \tag{4}$$

The resulting map of seismic strain rate is shown in Figure 5b. $\dot{\epsilon}$ is maximum in a region that is roughly 50 km away from the Alpine Fault on the eastern side of the Main Divide, and decreases away toward the divide and the Alpine Fault.

[15] It is worth noticing that, in this part of the orogen, the Alpine Fault which accommodates most of the relative motion between the Australian and Pacific plates is, for the most part, aseismic on a human timescale (Figure 5). This is commonly interpreted as indicating that most of the motion on the fault is accommodated by aseismic creep or by very large and infrequent earthquakes which have not been observed since settlement [*Allis*, 1986]. Today there is still no conclusive observation that clearly indicates the (non)occurrence of great earthquakes on the Alpine Fault. This topic is still vigorously debated [e.g., *Allis*, 1986; *Walcott*, 1998; *Beavan et al.*, 1999; *Norris and Cooper*, 2000] and the seismic strain rate calculated here cannot, in any case, be used to infer the seismic behavior of the Alpine Fault.

[16] The gradual decrease in seismic strain rate amplitude from its maximum value on the eastern flanks of the orogen indicates that the brittle deformation is indeed confined to the proshears on the eastern side of the orogen. The low seismic energy release on the western side of the divide clearly suggests that the same faults are passively advected toward the divide and the western side of the orogen where faulting thus plays little or no role in controlling the development of the major topographic features. The asymmetry in seismic energy release across the divide thus supports the suggestion made by *Koons et al.* [2002] that it is faulting that controls the geomorphology on the eastern side of the orogen by producing relatively large topographic gradients/steps that lead to the formation of large glacial valleys and their drainage basins, while, on the western side of the divide erosion dominates and the structural controls vanishes. The valleys created by reverse faulting near the eastern edge of the orogen deepen as they move laterally toward the divide, mostly through glacial erosion or further faulting. Ultimately these valleys are transported across the divide and subjected to a radically different environment in which erosion is controlled by glacial and fluvial processes and where the mean tectonic uplift rate is ten times greater.

4. Fluvioglacial Landscapes Throughout the Southern Alps

[17] *Adams* [1980] was first to point out that the main characteristics of the landscape in the Southern Alps result from the combined action of fluvial and glacial erosion, alternating through glacial cycles. He suggested that while glacial erosion may deepen and widen valleys, it removes little material from the valley slopes, whereas interglacial erosion concentrates on valleys walls. *Whitehouse* [1987] divided the landscape of the Southern Alps in 3 different regions: (1) an ''old glacial landscape'' on the southeastern side of the mountain range, (2) in the central part, a recently glaciated landscape (characterized by the presence of steep backwalled cirques) and (3) a fluvially dominated landscape on the western side of the Main Divide (where V-shaped valleys have formed in response to intense fluvial dissection, landsliding, and rockfall–snow avalanching). More recently, *Hovius et al.* [1997] described the western side of the mountain belt as characterized by ''dissected, rectilinear slopes, frequently steeper than 45° and with thin (<1 m) regolith cover'' where the dominant mass transport mechanism is landsliding triggered by bedrock channel incision.

[18] This division of the landscape is clearly seen in the character of the main trunk valleys and in the shape of the interfluves. On the eastern side of the divide, the landscape is built around a series of large, linear, U-shaped, deeply carved and partially filled glacial troughs (Figure 6a) and the interfluves are characterized by relatively low drainage density networks composed of mostly linear segments and rectangular drainage basins. The landscape is clearly dominated by glacial features. On the eastern side of the orogen, the position of the ELA during the four late Pleistocene ice advances has been estimated at between 500 and 1000 m below its present-day value [*Porter*, 1975]. The lack of evidence for interglacial fluvial reworking is to be attributed to the relatively low precipitation rate resulting from the strong orographic control on precipitation and the gentler slopes characterizing that side of the orogen. There is also a progressive variation from a fully glaciated landscape in the north to more fluvially dominated landforms in the south as documented along the Ben Ohau range by *Kirkbride and Matthews* [1997] and *Brocklehurst* [2003].

[19] On the western side of the divide, the interfluves are characterized by a much greater drainage density than on the eastern side of the divide and channel networks are clearly dentritic (Figure 6a). The main trunk valleys have a more complex morphology alternating between glacial troughs near the divide, deeply incised V-shaped valleys at midelevations and flat-bottomed, low-elevation (close to sea level), gravel filled valleys where high-energy meandering channels transport a large load from the slopes of the mountain range to the nearby ocean (Figure 6b). This progression is illustrated in Figure 7 by a series of aerial photographs taken from an helicopter along the Whataroa River.

[20] To further illustrate this complexity of the landscape, we show a high-resolution satellite image (Advanced Spaceborne Thermal Emission and Reflection Radiometer (ASTER)) of the Whataroa River, the downstream profile (thalweg) of the river derived from a 50 m digital elevation model, a series of four valley cross sections as well as estimates of local slopes (Figure 8). Near the divide, the valley floor is still partly covered with ice (Figure 8a), the valley cross section is clearly U shaped (Figure 8h) and the upper reaches of the river correspond to a glacial cirque backwall (Figure 8b). This section of the river has clearly been shaped by glacial processes. The extent of this 'young glacial landform' can be appreciated by considering the distribution of local slope (Figure 8d) where the sharp glacial ridge crests dominate the landscape at high elevation. The middle section of the river is characterized by deeply incised V-shaped valleys flanked by rectilinear slopes (Figured 8f and 8g). The river profile (Figure 8b) and the valley cross sections are clear evidence of bedrock incision by fluvial processes. The rounded tops of the interfluves (Figure 8d) indicate that landsliding is the dominant mode of mass transport along hillslopes as clearly demonstrated by *Hovius et al.* [1997] and illustrated in Figure 8i. Locally, near the confluence with a large tributary (here the Butler River), the valley widens and the river briefly meanders on a relatively flat, gravel-filled bed. The origin of these debris may be related to the formation of an oversteepening of the main trunk valley at the confluence between two fast-flowing glaciers during glaciated times, as suggested by *MacGregor et al.* [2000]. Finally, the lower section of the Whataroa River is characterized by a flat-bottomed valley floor (Figure 8d) at a mean elevation close to sea level (Figure 8b) where the river forms large meanders (Figure 8a). This section of the valley is currently filled with up to several hundred meters of glacial debris as determined by a recent seismic survey near the mouth of a river nearby southwest of Fox Glacier (T. Stern, personal communication, 2005).

[21] Following *Whitehouse* [1987], the most obvious interpretation of these features of the landscape is that, although the landscape is mostly ice-free and the dominant mode of landform creation is currently fluvial, the region around the Whataroa River (and thus most of the western side of the orogen) is in a transitional state between glacial

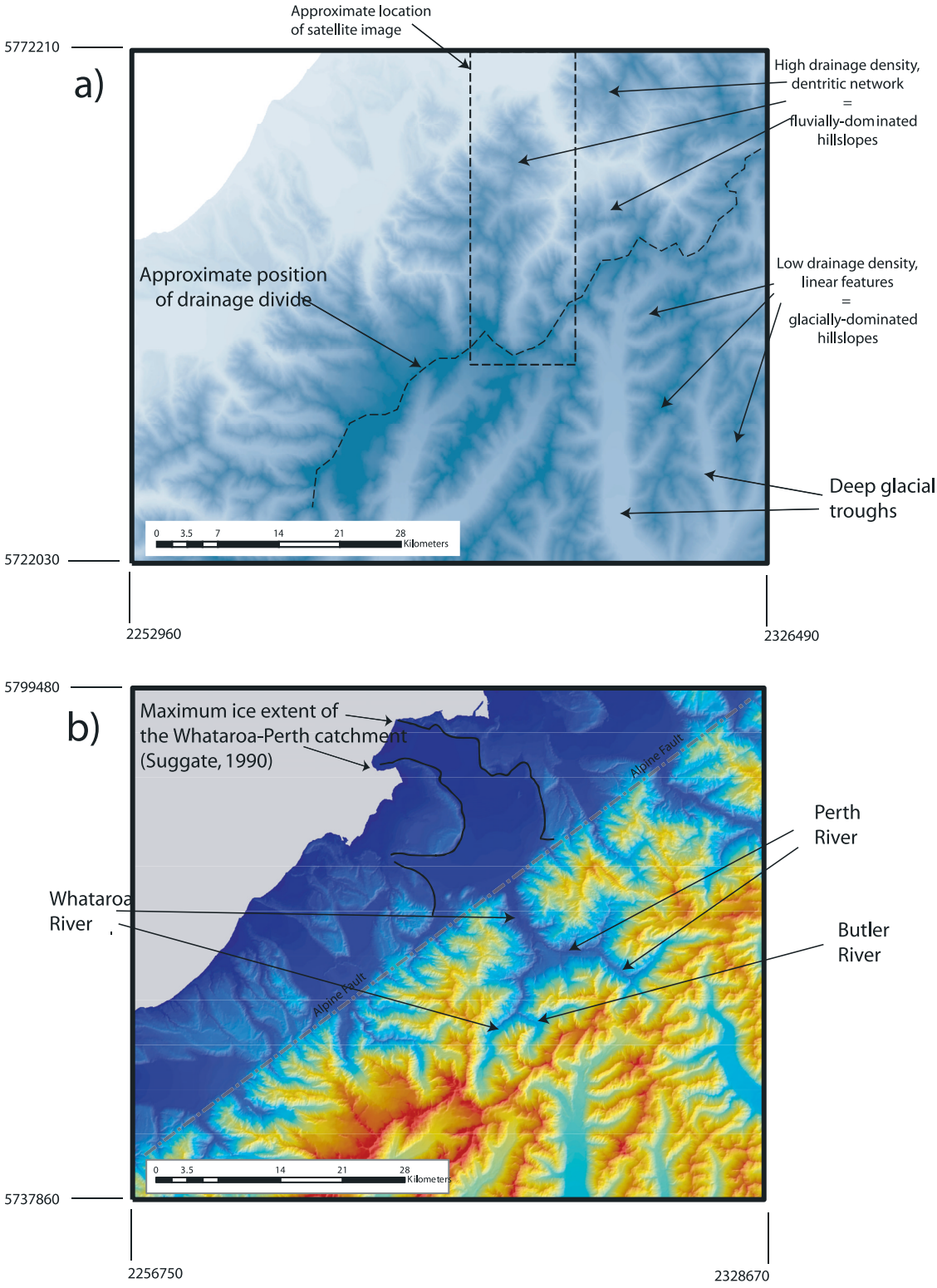

Figure 6. (a) Gray contours of elevation from the digital elevation model illustrating the difference in drainage density and character across the Main Divide. The dashed lines show the coverage of the satellite image presented in Figures 7 and 8. (b) Shaded color-contour map of elevation from a 50 m digital elevation model. The Whataroa and its main tributaries, the location of the Alpine Fault, and the maximum ice extent are shown.

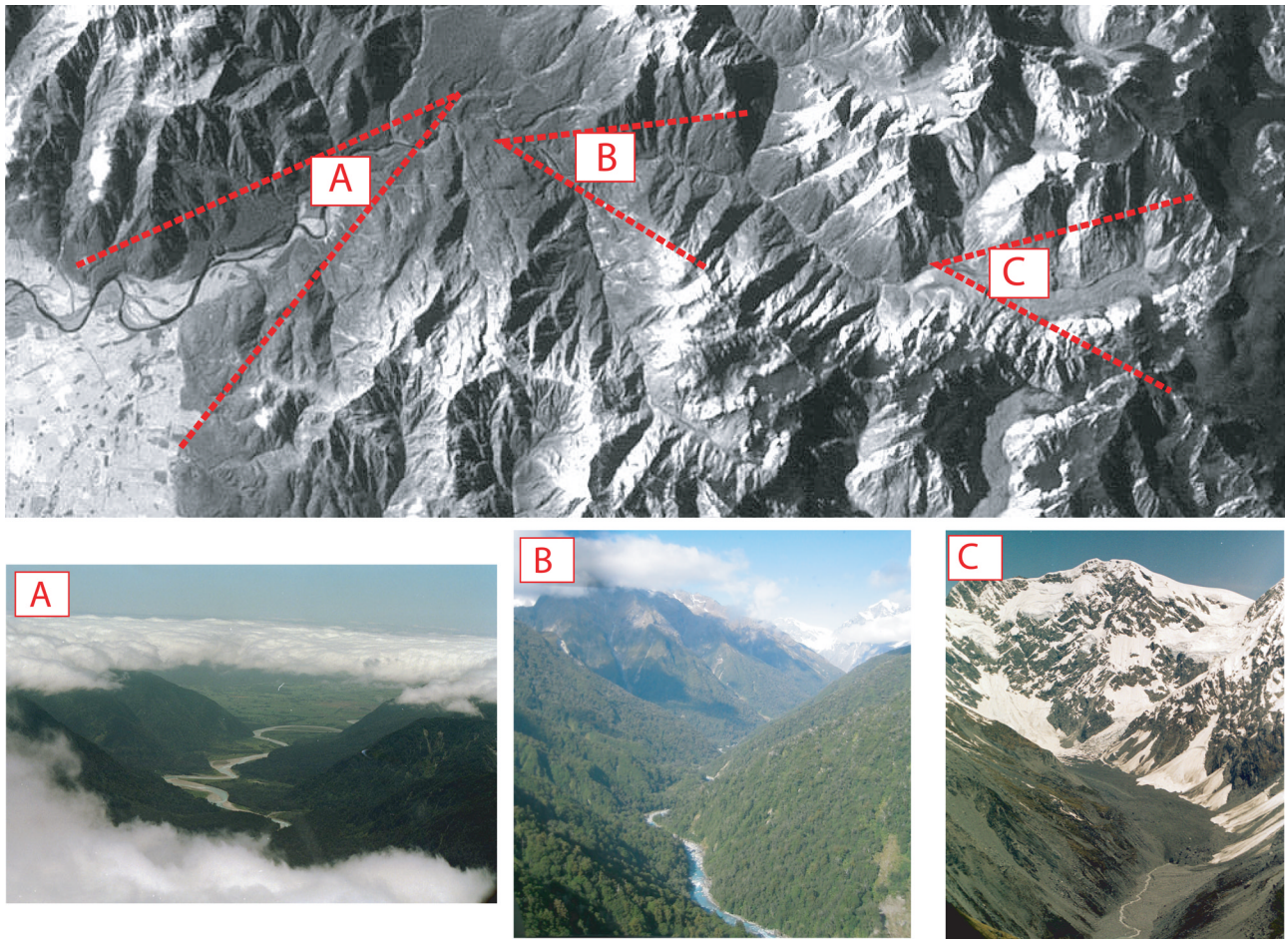

Figure 7. (top) Satellite image (ASTER) and (bottom) photographs of the landscape along the Whataroa River, illustrating the variations in landform described in the text: In the lower section (A), the valley is wide and the river meanders; in the middle section (B), the valley is narrow, flanked by steep, linear valley walls, and the river incises the bedrock; and in the upper reaches (C), the valley floor is still partly covered with ice, and the valley cross section is U shaped.

and nonglacial forms. It is clear that a large glacier flowed down the Whataroa valley during the last glacial period, as evidenced by the overdeepening of the valley near its intersection with the Alpine Fault, the presence of Holocene and Pleistocene moraines, and other glacial relicts [*Porter*, 1975; *Willett*, 1950; *Adams*, 1980; *Whitehouse*, 1987; *Suggate*, 1990]. We highlight in Figure 6b the position of the maximum ice extent (latest Otira glaciation, ~14,000 yr ago [*Suggate*, 1990]). Interestingly, where the river crosses the Alpine Fault no alluvial fan is observed. This confirms that the ice has carved the valley below sea level, which has in turn been filled as a consequence of the ice retreat as suggested by *Whitehouse* [1987].

[22] The whole area is currently uplifting at a rate of 8 to 12 mm/yr, which results in approximately 1 km of mean rock uplift over the last glacial cycle or 100–200 m since the end of the last glacial period. Because the orogen remains relatively modest in size (the mean topographic elevation near the divide is less than 3000 m), this extremely fast uplift rate must be compensated by a similar erosion rate. This rapid uplift and the extreme precipitation rate characterizing the area (locally up to 13 m/yr) have com-

Figure 8. (a) Satellite picture (ASTER) of the Whataroa River area. (b) River profile derived from the digital elevation model (DEM) shown in Figure 8c as well 1-D modeled longitudinal profile; note that the horizontal coordinate is easting, not down-profile distance, for easier comparison with Figures 8c and 8d. (c) Topography derived from 50 m DEM. The thin red lines are stream locations derived by computing the path of steepest descent (maximum slope) from five selected points on the DEM; in regions of low gradient, DEM resolution may lead to the stream following a negative slope and the formation of lake-like areas. (d) Norm of the gradient vector (or maximum slope) expressed in degrees and calculated from the 50 m DEM. (e–h) Valley cross sections derived from the DEM; locations are shown in Figure 8c. Note that the vertical exaggeration varies between the different valley cross sections and the longitudinal profiles. (i) Distribution of landslides as given by *Hovius et al.* [1997] superimposed on Figure 8a.

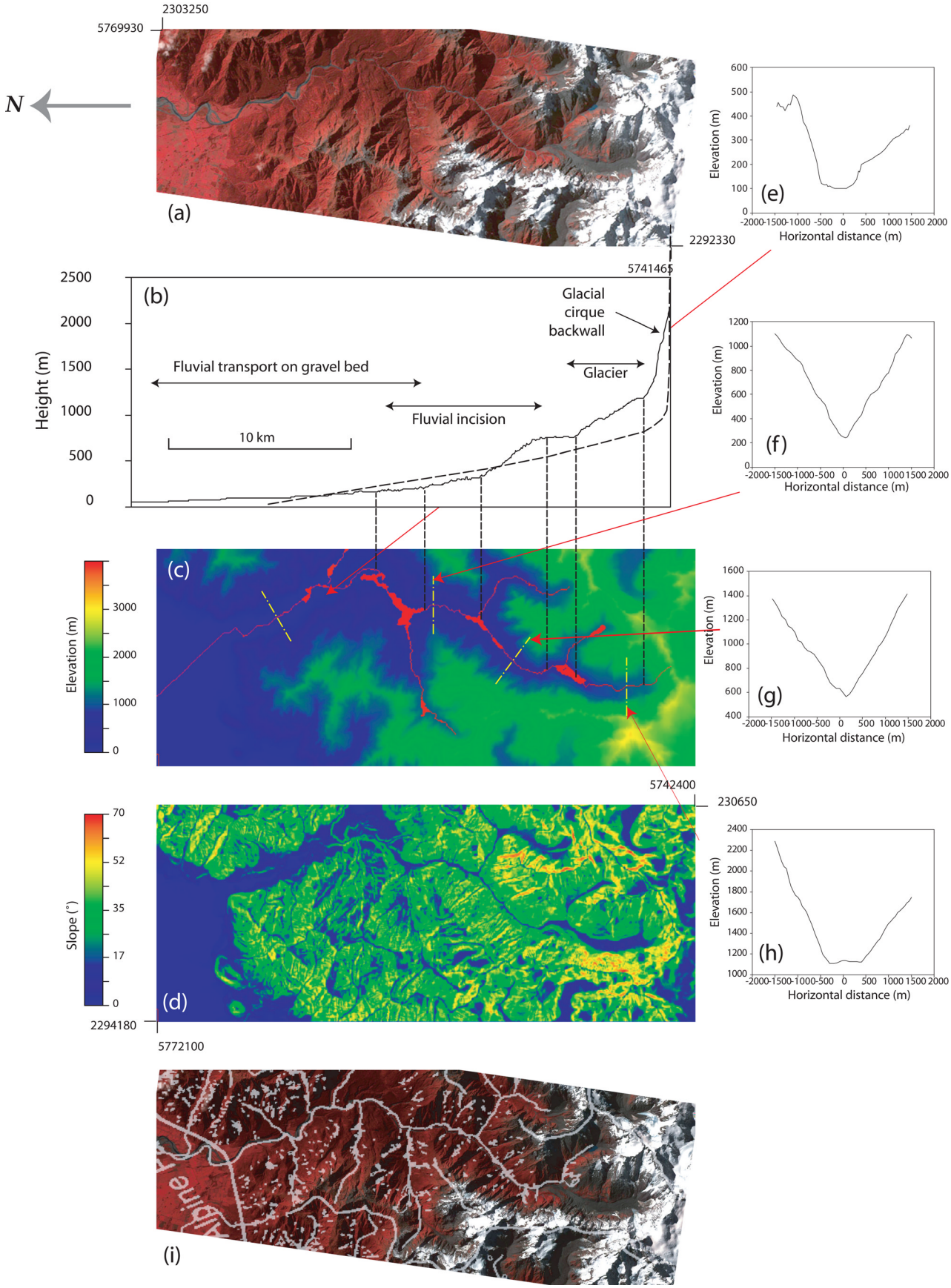
2303250
5769930
N
(a)
2292330
5741465
(b)
Height (m)
2500
2000
1500
1000
500
0
Glacial cirque backwall
Fluvial transport on gravel bed
Glacier
Fluvial incision
10 km
(c)
Elevation (m)
3000
2000
1000
0
5742400
230650
Slope (°)
70
52
35
17
0
(d)
2294180
5772100
(i)
(e)
(f)
(g)
(h)
Elevation (m)
Horizontal distance (m)
-2000 -1500 -1000 -500 0 500 1000 1500 2000

Figure 8

bined to transform most of the glacial form into a fluvially dominated landscape. Two regions have not yet recovered from the glacial period: the upper part of the western face of the mountain range that is still partly covered in ice, and the lowest section of the valley floor that is still filled with up to 600 m of glacial debris which is progressively uplifted and transported away by the high-energy river.

[23] The timing and extent of glaciation within each catchment have yet to be accurately constrained, which makes it difficult to determine what fraction of the basin has seen a glacial state in the last 100 kyr. Dating of moraines [e.g., *Suggate*, 1990] show that the last glaciation culminated between 28 and 18 kyr ago. The geometry of the mountain range, the high precipitation rates and climate history, which strongly controls the regional mass balance of the ice cap, suggest a very rapid and massive retreat beginning ~14 kyr ago which quickly led (by 12 kyr) to an ice volume close to the one observed today [*Suggate*, 1990].

5. Geomorphic and Tectonic Models

[24] In the following sections, we present the fundamental equations that are commonly used to parameterize large-scale landforming processes. We then present a simple parameterization of the tectonic collision presently occurring in South Island, New Zealand, based on our current understanding of the geometry and relative convergence velocity between the two colliding plates.

[25] These equations are combined and solved in one dimension, to isolate the role of bedrock incision on the dynamics of the drainage divide. We then move to a 2-D solution to explore the effect of hillslope erosion, focusing on the fluvial response of the landscape after a period of glaciation.

5.1. Geomorphic Model: Fluvial and Hillslope Erosion

[26] Following previous geomorphic models [*Davis*, 1892; *Beaumont et al.*, 1992; *Chase*, 1992; *Braun and Sambridge*, 1997], we assume that large-scale landform evolution on tectonic timescales is controlled by two main surface processes: (1) diffusion of hillslope topography (i.e., processes controlled by local slopes) and (2) incision of bedrock by fluvial channels. Diffusion represents a range of processes, for example, weathering, slope wash, overland flow and soil creep as well as mass wasting by bedrock-involved landsliding, which are difficult to explicitly and independently model at the scale of a mountain belt and are commonly parameterized through a simple linear diffusion equation [e.g., *Davis*, 1892; *Gilbert*, 1909; *Koons*, 1987; *Beaumont et al.*, 1992; *Braun and Sambridge*, 1997; *Herman and Braun*, 2006]:

$$\frac{\partial h}{\partial t} = -D\nabla^2 h \tag{5}$$

where h (m) is the altitude, t the time (yr) and D is the diffusivity (m^2/yr). *Braun et al.* [2001] and *Herman and Braun* [2006] have shown that on soil-covered hillslopes, linear soil creep is the dominant transport mechanism along the steeply dipping sections of the hill sides whereas depth-dependent, nonlinear soil creep is more likely to be efficient in regions of soil accumulation near the bottom of hills, in part justifying the use of a linear diffusion equation to represent erosion by weathering and soil transport along steep valley walls. It is clear, however, that in active tectonic areas, landsliding is a major contributor to mass transport from steep valley sides to valley bottoms, especially in oversteepened, U-shaped glacial valleys [*Hovius et al.*, 2000]. Landsliding has been parameterized by a nonlinear form of the diffusion equation [*Roering et al.*, 2000] or by introducing a critical slope [*Schmidt and Montgomery*, 1995; *Densmore et al.*, 1998]. We feel, however, that it is inappropriate to introduce explicitly landsliding in our 2-D landscape evolution model because its spatial resolution is insufficient to represent slopes in excess of 30°–40°. At this stage, it is not computationally viable to do so, especially if one is interested in landscape evolution at the scale of an active orogen, and it is more appropriate to represent hillslope landsliding within a simple diffusion term in the equation governing geomorphic processes, keeping in mind that its efficiency (i.e., the diffusivity) needs to be scaled appropriately.

[27] Along valley floors, channel incision is most efficient at lowering topography and is often parameterized by function which is assumed to take a power law form [e.g., *Howard*, 1994; *Whipple and Tucker*, 1999]:

$$\frac{\partial h}{\partial t} = -KA^m(\nabla h)^n \tag{6}$$

where K (m^{1-2m}/yr) represents a dimensional coefficient of erosion, A is drainage area, used as a proxy for local discharge, ∇h is the river gradient (in the direction of water flow), and m and n are positive constants. The coefficient K is commonly assumed to be influenced by many climate-related factors including precipitation, storminess as well as sediment flux, lithology or channel width [e.g., *Whipple and Tucker*, 1999].

5.2. Tectonic Model

[28] Continental collision is the end product of the closure of an oceanic basin by subduction along one or both of its margins. An orogeny can therefore be regarded as being driven by a subduction-accretion mechanism in which the main driving force is the shear stress imposed by the subducting mantle lithosphere [*Davis et al.*, 1983; *Willett et al.*, 1993; *Beaumont et al.*, 1994; *Braun and Beaumont*, 1995] as opposed to the horizontal force imposed by an indentor [*Molnar and Taponnier*, 1975]. The critical wedge theory [*Davis et al.*, 1983] has been proposed in order to capture the simple geometry of an accretionary prism, using the assumptions that the entire wedge is deforming in response to basal traction and is at plastic failure. It predicts that surface slope is maintained by ongoing material accretion resulting from underthrusting of stronger material beneath the wedge. This simple model has been applied to the scale of an orogenic belt [*Willett et al.*, 1993]. Numerical and analog models have shown that the deformation need not to be uniformly distributed across the wedge but is more likely to be accommodated by discrete faults. Furthermore, when basal traction results from the velocity discontinuity imposed at the base of the crust by the subduction of the underlying mantle, a second critical taper forms that dips in the opposite direction. Conse-

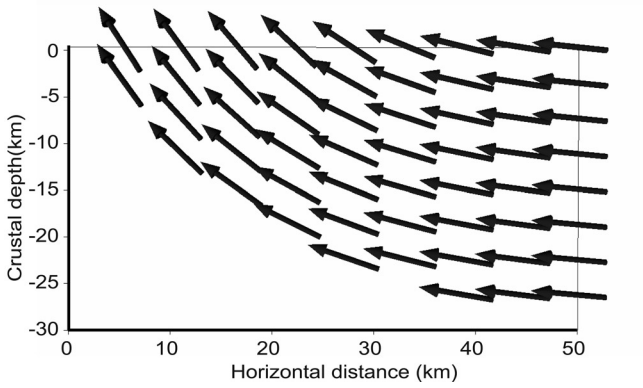

Figure 9. Kinematic model used to represent the convergence in the tectonomorphic model developed here and derived from the "rule of the normal" [*Braun et al.*, 1994].

quently, a set of oppositely dipping shear zones develops resulting in uplift of a "triangular plug" between the two shears. This mode of deformation is known as the "doubly vergent critical wedge" model. The orogen-scale geometry of this model is summarized in Figure 2a from [*Batt and Braun*, 1999]. The accreting side is defined as the "proside" and its opposite as the "retroside," adopting definitions introduced by, for example, *Willett et al.* [1993]. In cases where accretion and erosion operate simultaneously, rocks are advected into the orogen from the so-called proside, accreted across the proshear and are then thrust up along the retroshear and exposed at the surface of the orogen.

[29] In this paper, we parameterize the first-order characteristics of the deformation patterns within a doubly vergent wedge representing an actively deforming/accreting orogen by making use of a two-dimensional velocity distribution (or kinematic representation of rock paths) that assumes the retrothrust is linked to the basal subhorizontal detachment between the crust and the underlying mantle to form a unique structure. The geometry of this single structure is represented by the following expression:

$$z(x) = -z_0[1 - \exp(-x/\lambda)] \tag{7}$$

where z_0 is the depth of the detachment and λ (km) the listricity of the retroshear. Note that, in this parameterization, the surface dip of the retroshear is given by z_0/λ. The velocity of rocks that are brought into the orogen by the convergence between the two plates is assumed not to vary in amplitude along the fault. This can be interpreted as assuming that the fault (or shear zone) is effectively very weak or frictionless. To constrain the velocity field within the accretionary belt, we make use of the "rule of the normal." This rule assumes that there are lines in the hanging wall which remain normal to the fault both prior to and following deformation [*Braun et al.*, 1994]. The resulting velocity field (Figure 9) is very similar to that proposed independently by *Wellman* [1979] and is commonly used to represent particle paths in the Southern Alps [*Beaumont et al.*, 1996b; *Batt and Braun*, 1999]. The value of the parameters (v_h = 8 mm/*yr*, z_0 = 26 km and λ = 22 km; where v_h is the horizontal convergence velocity) have been constrained using thermochronological data, that is, fission track and K-Ar data [*Kamp and Tippett*, 1993; *Batt et al.*, 2000; Herman et al., submitted manuscript, 2005].

5.3. Tectonomorphic Model

[30] Combining equations (5) and (6) with the tectonic model, we obtain the following general equation:

$$\frac{\partial h}{\partial t} = u_u - v\frac{\partial h}{\partial x} - KA^m(\nabla h)^n - D\nabla^2 h \tag{8}$$

where u_u is the vertical uplift velocity and v represents the horizontal velocity in the x direction induced by the continental collision. In our case, both velocities are derived from the rule of the normal applied to equation (7). Note that we have neglected the component of the velocity field parallel to the strike of the main thrust. In the Southern Alps, the relative velocity between the two colliding plate is strongly oblique to the strike of the Alpine Fault. However, *Tomkin* [2000] demonstrated that the effects of the three-dimensionality of the tectonic velocity field are almost negligible on the evolution of the geomorphic system since most of the strike-slip deformation is taken up on the Alpine Fault [*Beavan et al.*, 1999].

5.4. Position and Height of the Drainage Divide: 1-D Model

[31] First we explore the behavior of the tectonomorphic system by investigating how bedrock incision may control the position and height of the drainage divide. To do so, we simplify equation (8) to its one-dimensional form, in the direction of tectonic convergence, that is, perpendicular to the strike of the main thrust. This leads to the following equation for h, the height of surface topography:

$$\frac{\partial h}{\partial t} = u_u - v\frac{\partial h}{\partial x} - KA^m\left(\frac{\partial h}{\partial x}\right)^n - D\frac{\partial^2 h}{\partial x^2} \tag{9}$$

where A, the drainage area, is assumed to be linearly proportional to $x - x_d$, and x_d is the position of the water drainage divide. These approximations enable us to keep the problem simple and isolate each of the various processes; in particular we are interested in quantifying the effect of orographic precipitation by applying different erosion rates on either sides of the drainage divide. This is a simple representation and the quantitative results must be interpreted carefully. However, the qualitative behavior of the system described here remains valid.

[32] A finite difference scheme is used to solve equation (9) on a regular grid (Δx = 100 m). The divide position is defined as the intersection of two river profiles, flowing on each side of the mountain belt, and is assumed to lie between two integration points such that drainage area is never exactly equal to zero, even for points at or near the drainage divide. The time dependency is treated explicitly. The time step is taken small enough (1 yr) to ensure numerical stability and accuracy. At each time step, equation (9) is treated in two steps. First, the horizontal advection and vertical uplift terms are solved using a total variation diminishing (TVD) algorithm [*Finlayson*, 1992] optimally designed to solve the transport equation of moving fronts. In this way, we can control numerical instabilities generated at the topographic discontinuity

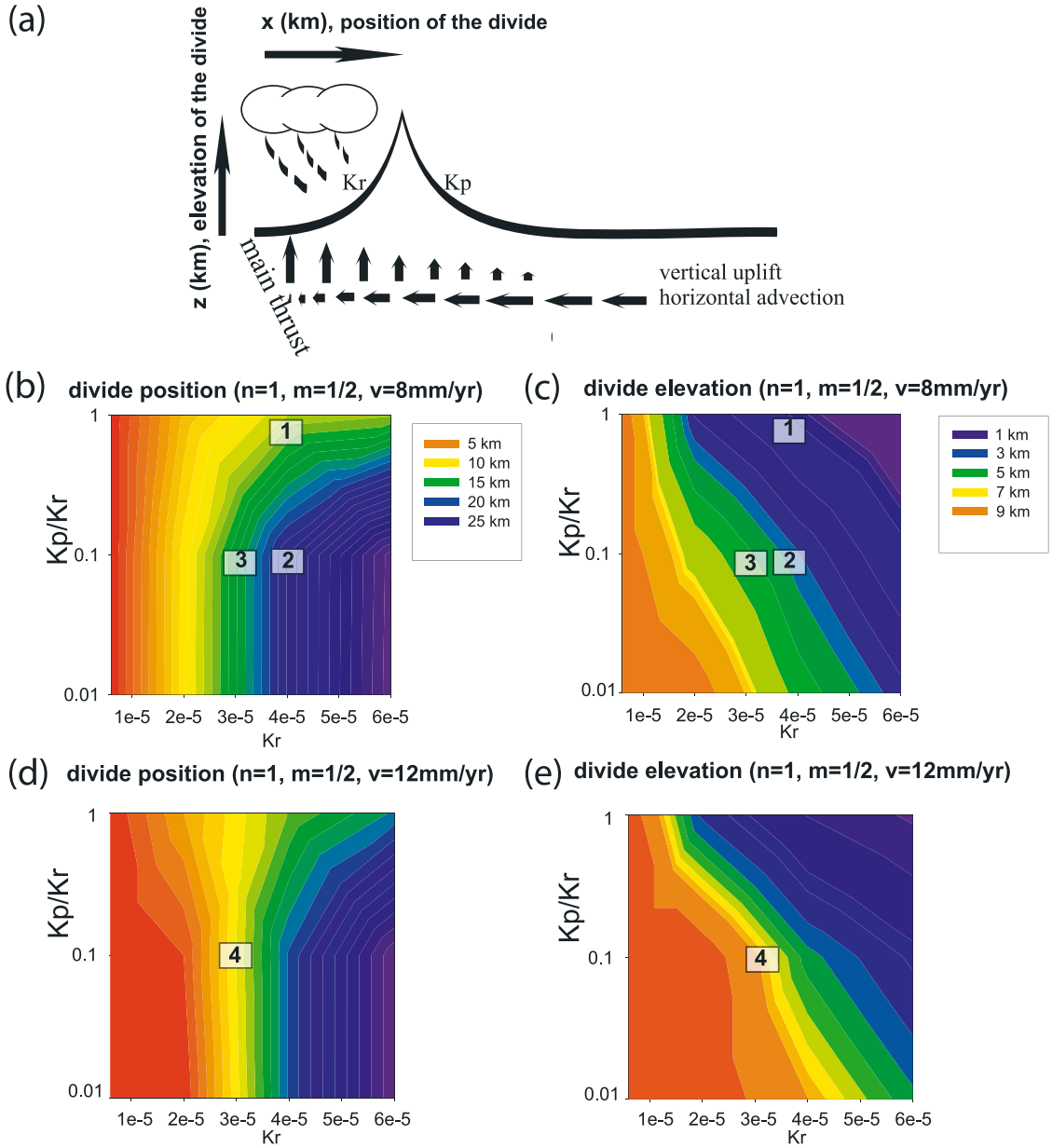

Figure 10. (a) One-dimensional (1-D) model setup. (b–e) Results from the 1-D model as contour plots of the drainage position (Figures 10b and 10d) and height (Figures 10c and 10e) in parameter space [K_r, K_p/K_r]. The numbers indicate the position in parameter space of the various model runs shown in Figure 11.

corresponding to the drainage divide. Secondly, the fluvial erosion and diffusive terms are solved using a finite difference scheme alternating between upwind and backward difference depending on the sign of the local slope. All numerical experiments are initiated with a small topography to ensure the existence of a drainage divide at the start of the experiment and proceed until a topographic steady state is reached, that is, $\frac{\partial h}{\partial t} \simeq 0$. In practice, we stop the experiment when the divide migration velocity is less than 1 mm/yr. This typically takes place within 1 to 3 Ma from the start of the experiment, depending on how far from steady state the initial conditions are set. For each model, the horizontal and uplift velocities and the fault geometry are assumed to remain constant; that is, there is no assumed feedback from erosion to tectonics.

[33] Results are summarized in Figure 10. To construct each parameter map, we run 12 models within the reported parameter limits (Figure 10). We investigate the model response to changes in K and v (v and u_u are linked through the tectonic model and mass conservation). To appraise the orographic effect, we test the effect of using different values for K on the retroside (K_r) and proside (K_p) of the water drainage divide. Because our study is focused on the behavior of the Southern Alps of New Zealand where the orographic effect is strongest on the western side of the orogen, we consider cases where $K_p/K_r \leq 1$ only. We

Table 1. One-Dimensional Model Parameter Values

Parameter	Model 1	Model 2	Model 3	Model 4
K_r, $km^{1-2\ m}/yr$	4E-5[a]	4E-5	3E-5	3E-5
K_p/K_r	1.00	0.10	0.10	0.10
D, km^2/s	1E-12	1E-12	1E-12	1E-12
m	1/2	1/2	1/2	1/2
n	1	1	1	1
v, km/yr	8E-6	8E-6	8E-6	12E-6

[a]Read 4E-5 as 4×10^{-5}.

impose a very small value of D (1e−12 km^2/yr) to stabilize the numerical procedure near the divide. At steady state, equation (9) becomes

$$u_u - v\frac{\partial h}{\partial x} \simeq KA^m\left|\frac{\partial h}{\partial x}\right|^n \tag{10}$$

which represents the balance between the tectonic and fluvial erosion terms.

[34] In the first set of experiments (Figures 10b and 10c), we vary K_r as well as the ratio K_p/K_r. The power law exponents are set to $m = 1/2$ and $n = 1$. In a second set of experiments (Figures 10d and 10e), the convergence velocity is increased from 8 to 12 mm/yr. All other parameters are kept constant at a reference value given in Table 1.

[35] The results of the model show that the position of the divide is very sensitive to the fluvial erosion efficiency (K_r). The more efficient fluvial erosion, the farther away the divide is from the fault. There is also a clear dependence on the orographic precipitation. As the precipitation becomes more asymmetrical, the divide's equilibrium position becomes more distant from the fault. Finally, there is a mild dependence on the convergence velocity. As the velocity increases, the divide moves closer to the fault; one could state that the divide is, in a way, advected by the tectonic velocity. The divide height is inversely proportional to fluvial erosional efficiency, directly proportional to the degree of asymmetry in precipitation and to the convergence velocity.

[36] To understand the behavior of the model, we now consider how each term of equation (10) contributes to the steady state balance, first for a ''reference run'' (labeled 1 on Figures 10b and 10c) in which there is no orographic control to precipitation ($K_p = K_r$), then for a series of three other model runs in which one of the parameters is changed. For each of these model runs, the steady state topographic profile is shown in Figure 11a, while the contribution to the erosion rate or uplift rate from each of the terms of equation (10) is shown in Figures 11b–11e.

[37] In the reference model run (model 1, Figure 11b), surface uplift is everywhere balanced by fluvial erosion, except near the divide where the advection term plays a finite, apparently minor role. Because of the opposing slopes on either side of the divide, the advection term contributes to tectonic uplift on the retroside of the orogen, while, on the proside, it acts as a subsidence (or erosion) term. Variations in divide position should therefore preferentially affect the topographic balance through the advection term.

[38] Introducing asymmetry in the model precipitation leads to a clear migration of the equilibrium position of the divide away from the fault (model 2, Figure 11c). This is the only way by which the system can cope with the high erosion rate imposed. As the divide migrates away from the fault, a greater proportion of the part of the orogen that is subjected to high uplift rate is on the retroside (or wet side) of the orogen. The final position of the divide is also controlled by the contribution of the advection term to the topographic balance on the proside of the orogen where fluvial erosion plays a rather minor role in the topographic balance. The divide is pinned at a location where the uplift term is large enough to compensate the advection term. Ultimately, in a case of no fluvial erosion (extreme orographic effect), the tectonic uplift should be perfectly balanced by the advection term. This case corresponds to a surface that is progressively uplifted and advected toward the divide without any erosion. The divide location is therefore controlled by the kinematics of the tectonic model.

[39] Decreasing the mean fluvial efficiency (i.e., on both sides of the divide), leads to a migration of the divide's position toward the fault (model 3, Figure 11d). Because precipitation is asymmetric, decreasing the fluvial efficiency on both sides of the divide leads to a greater decrease in fluvial erosion on the retroside than on the proside. To maintain the balance with the tectonic uplift, the divide must move closer to the fault, to increase the contribution to uplift from the advection term on the retroside and increase the contribution to subsidence from the advection term on the proside. This result therefore demonstrates that it is the contribution of the advection term to the overall topographic balance that controls the position of the divide in response to changes in mean fluvial erosion efficiency.

[40] Similarly, increasing the convergence velocity causes the divide to migrate toward the fault (model 4, Figure 11e) in such a way that both the fluvial and advection terms on the proside of the orogen balance the tectonic uplift term. In all cases where orography is asymmetric, the position of the divide is controlled by the balance between fluvial erosion, advection and uplift on the proside of the orogen. The low fluvial efficiency on the proside limits the potential for slope change and therefore the advection term plays a significant role in the topographic balance. Contrary to that, the fluvial erosion term dominates the topographic balance on the retroside and sets the shape of topography (slope) to balance uplift. This behavior is also confirmed by the clear proportionality between the height of the divide and its position from the fault (Figure 11a) along a quasi self-similar profile.

[41] We compare our results to those obtained by *Willett et al.* [2001] by calculating a similar dimensionless ratio. We estimate the value of the fractional divide position (i.e., $F_D = \frac{50-x_d}{50}$) and plot it against the ratio K_p/K_r (Figure 12a) and the velocity ratio R, that is, $\frac{v}{u_u}$ (Figure 12b). Contrary to work by *Willett et al.* [2001], v and u_u are dependent and R varies across the orogen (minimum near the retroshear). The range of values we obtain is however similar to that of *Willett et al.* [2001] for both F_D and R. For small K_r, the divide position is mostly dependent on R, whereas when K_r increases the divide location, or F_D, is clearly controlled by both R and K_p/K_r. When K_p/K_r decreases the divide migrates toward the proshear. Ultimately, when there is no erosion on the proside the divide position is entirely controlled by R, that is, the kinematic conditions as stated above. This result complements the work of *Willett et al.* [2001] by illustrating

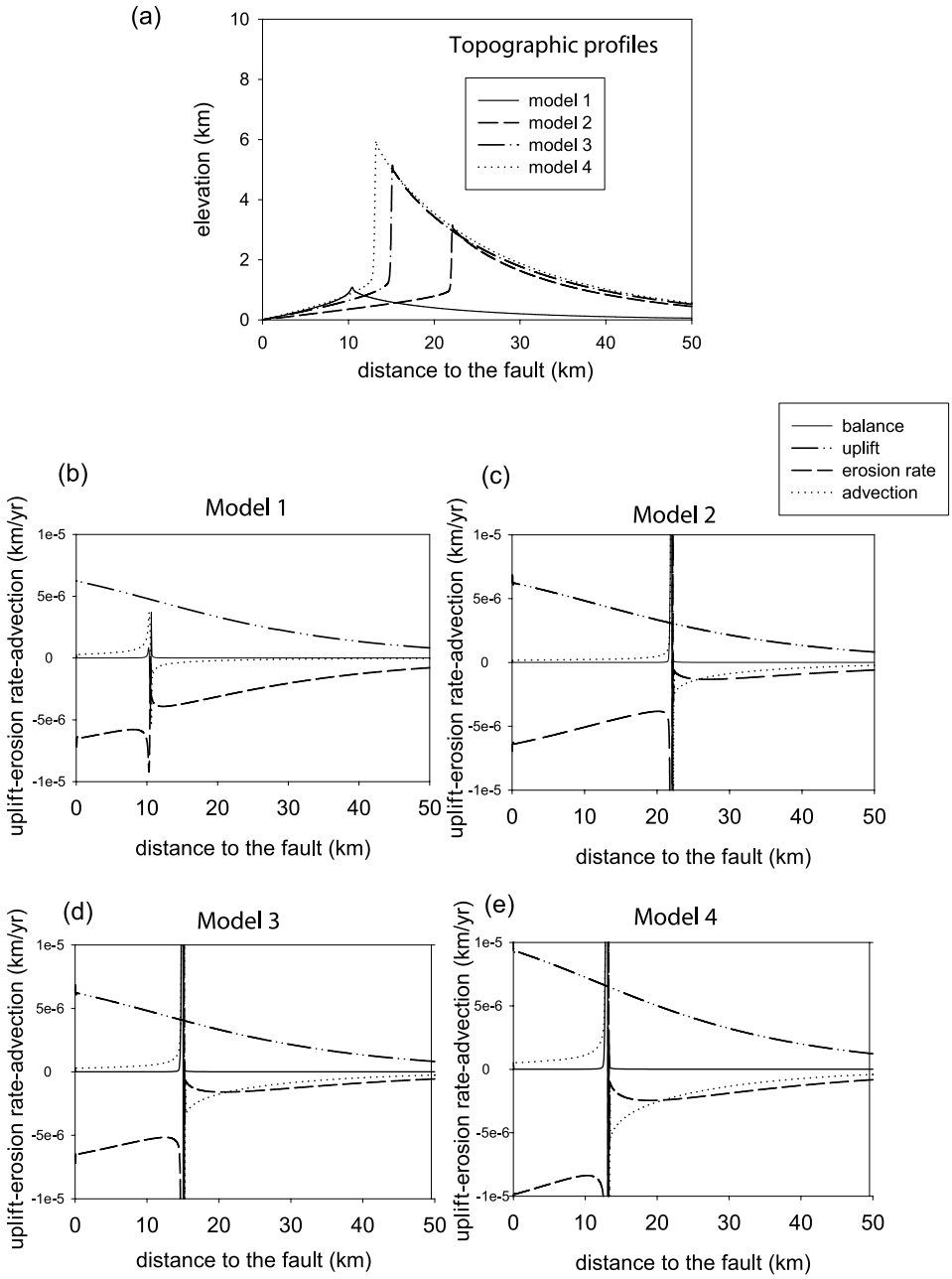

Figure 11. (a) Topographic profile predicted from four 1-D model runs. (b–e) Contributions to the topographic balance from each of the three terms in equation (10) (uplift is u_u, advection is $v\frac{\partial h}{\partial x}$, and erosion rate is $KA^m(\frac{\partial h}{\partial x})^n$).

how the orographic conditions, or the differential erosion rates on either side of a drainage divide, influence the process of divide migration. This suggests therefore that any variation of the efficiency of erosion on one side of the divide will cause the divide to change its location.

[42] The profiles computed from the 1-D model appear unrealistically steep near the divide (Figure 11a). The introduction of a slope threshold could remedy this problem but the value of the critical slope to use is difficult to chose. We have performed a large number of model runs in which a critical (maximum) slope was introduced. The behavior of the model, that is, its sensitivity to changes in precipitation asymmetry and uplift rate, is largely unaffected by the introduction of a critical slope; although the position of the divide becomes a function of the critical slope value, it is simply systematically shifted away from the coast by an amount that is linearly proportional to the imposed critical slope. It is however interesting to note that, in the Whataroa region for example, extremely steep slopes (60°–70°) exist near the divide as shown on Figure 8d. Furthermore, landsliding is uncommon in these parts of the landscape (as shown in the distribution of landslides in Figure 8i) making it difficult to select an appropriate value for the critical slope. We have thus chosen not to use a critical slope

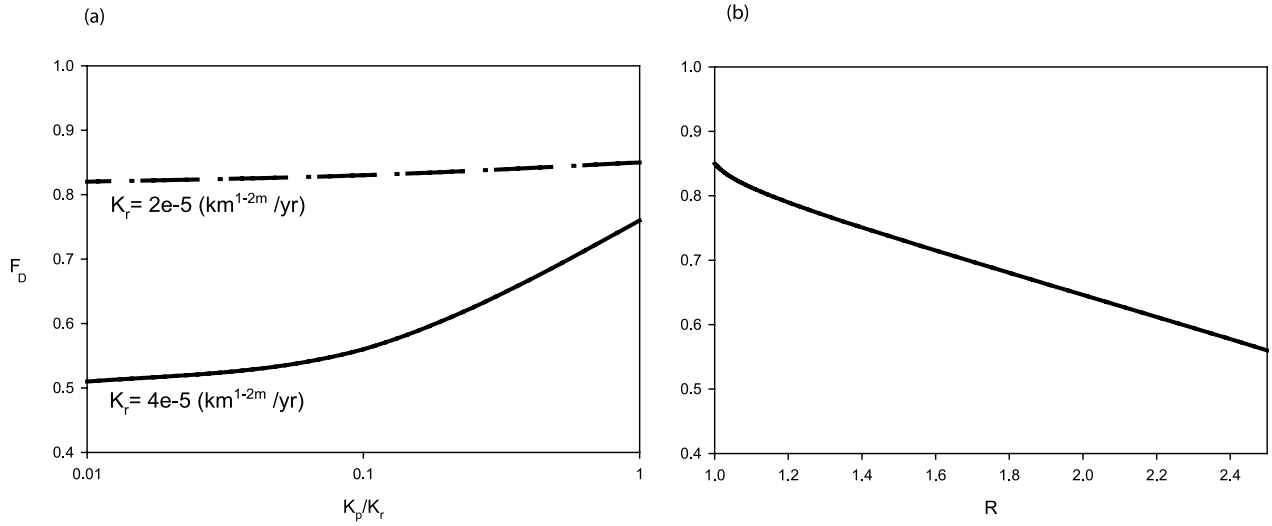

Figure 12. (a) F_D, the fractional divide position [*Willett et al.*, 2001], versus K_p/K_r at steady state. (b) F_D versus R, the velocity ratio $\frac{v}{u_u}$ [*Willett et al.*, 2001]; that is, for a given divide position we calculate the corresponding R.

in the results presented here. Finally, for the sake of comparison we have plotted one of the modelled profiles (model 2) against the Whataroa River profile (Figure 8b) to demonstrate that, although the slope of the synthetic profile is indeed too large in the vicinity of the divide, model predictions are consistent with the overall shape of the observed river profile.

5.5. Effect of Recent Glaciations: 2-D Model (CASCADE)

[43] We now turn our attention to the response of the landscape to recent changes in climatic conditions. We wish to determine which parts of the landscape are in steady state with the current climatic and thus fluvial erosional conditions and those that have not reached geomorphic steady state and are still recovering from the change in dominant erosional mechanism since the end of the last glaciation. To do so, we solve the two-dimensional version of the tectonomorphic model, equation (8), by using the landscape evolution model CASCADE developed by *Braun and Sambridge* [1997].

[44] We use the present-day topography of the west coast of the Southern Alps as initial starting geometry for the landscape and investigate where fluvial and hillslope processes are in equilibrium with the current landform by running CASCADE forward in time over a timescale of one thousand to one hundred thousand years. In CASCADE, the numerical mesh on which the differential equation is solved can deform with time. We have used this geometric flexibility to include the effect of horizontal tectonic advection. We have modified CASCADE by introducing cyclic boundary conditions on the sides of the computation domain that are parallel to the tectonic transport direction. The river network is constructed by connecting each node to its lowest natural neighbor [*Braun and Sambridge*, 1997] so that precipitation is collected and integrated downstream along the steepest local slope. Following this, each node of the grid can be assigned a water discharge, A, that is used to solve the fluvial erosion term in equation (8). The spatial resolution (1 km $\times$ 1 km nodes) is such that there is no need to distinguish between hillslope and channel elements as in the model of *Chase* [1992]. Using such a coarse grid also enables us to include the effect of bedrock landsliding within the diffusion term.

[45] Despite a large number of studies designed to constrain the rate parameters controlling basic geomorphic processes (i.e., K, D, m and n in our formulation), their values remain poorly constrained. Furthermore, these parameters vary with local climate and rock type; it is therefore difficult to determine universal expressions that could be used to derive their value in a given geologic and climate setting. Consequently, one cannot yet use landscape evolution model, such as CASCADE, as predictive tools, that is, using a well constrained set of parameter values. The approach used here is therefore based on a search through parameter space to investigate the behavior of the model and compare its response to climatic changes with that of the natural system. We limit our search to K, D and n and try to estimate what is the contribution to relief production/reduction of both bedrock incision and hillslope erosion during a postglacial period, although we realize that this may be an oversimplification of reality. We do not perform a search on m here and select it such that the concavity index (i.e., m/n) is 0.5 [*Whipple et al.*, 1999]. This is justified even though most river profiles are at disequilibrium because the values of the parameters m and n should be constant in a given setting and independent of the evolution of the system.

[46] To search through parameter space, we make use of the neighborhood algorithm (NA) [*Sambridge*, 1999a, 1999b]. This Monte Carlo type method is ideally suited to explore parameter space to find the minimum of a so-called ''misfit function'' by making use of geometrical concepts such as the natural neighbor and Voronoi diagram. The misfit function is usually defined as the difference between model predictions and observations. Here, we are interested in finding whether there exists a set of model parameters for which the landscape modifications

Table 2. Parameters Used in CASCADE

Parameter	RUN1	RUN2	RUN3
K, 1/yr	0.25	0.4	0.025
D, km^2/yr	5E-6[a]	0.29E-6	1E-6
u, km/yr	8E-6	8E-6	8E-6

[a]Read 5E-6 as 5×10^{-6}.

are minimized. Consequently, we use as a misfit function the following expression:

$$\chi^2 = \sum_i \frac{h(i) - h_0(i)}{h(i) + h_0(i)} \tag{11}$$

which is a true (i.e., statistically meaningful) χ^2 test measure of the difference between the initial h_0 and final h at each integration point i of the landscape. This test is performed in a bid to assess whether the topography calculated by the model can approach the actual topography. Minimization of this misfit function at all time would imply that the topography created by the model exactly corresponds to the present-day topography, at the scale of interest. Theoretically, if the system is at steady state (i.e., $\delta h = h(i) - h_0(i) = 0$, $\forall i$) an accurate parameterization should be found for short time runs, assuming that the physical model adopted is exact. In contrast, if the physical processes that created the landscape are different than those prescribed by the model (e.g., glacial erosion has been the main erosive agent, feedback mechanism between the surface processes and tectonics) no constraint on the parameters can be obtained. As time increases, a steady state would be reached if, and only if, the misfit function tends toward an asymptotic value. Note that in CASCADE, the computational grid points are advected with the imposed tectonic advection velocity (computations are made in a Lagrangian frame of reference). It is therefore necessary to interpolate the final solution onto the position of the initial landscape to estimate the misfit function. To perform this interpolation we use the natural neighbor interpolation which is consistent with the discretization used to solve the governing equations in CASCADE.

[47] Starting from the existing topography, we perform an inversion over four different timescales: 1, 10, 50, and 100 kyr. In doing so, we actually test whether the present-day topography is in steady state for fluvial and hillslope processes and/or how long it might take for the system to evolve toward steady state for different values of K, D and n.

[48] In all model runs, we use an initial topography that has been interpolated on a regular 1 km grid from a digital elevation model (GTOPO30, U.S. Geological Survey) using the natural neighbor interpolation. We selected a 50 $\times$ 50 km area along the Alpine Fault (Figure 1). CASCADE uses this grid to define the triangular mesh on which equation (8) is solved [*Braun and Sambridge*, 1997]. Note that we only use the part of the landscape that is on the western side of the Main Divide to construct the misfit function. This is because we know that the landscape of the east side of the divide is still partly covered by ice and is mostly glacial in character (Figure 6). The version of CASCADE that we have used permits us to advect the landscape horizontally but does not include a parameterization of glacial erosion. Details of the different model runs are summarized in Table 2. The time step is taken small enough to ensure numerical stability (100 years).

[49] The results of the NA search are shown in Figure 13. Each dot represents the position of a forward run of CASCADE in the parameter space. The color scheme used is based on a percentile value which corresponds to the ratio of the difference between the forward run misfit value and

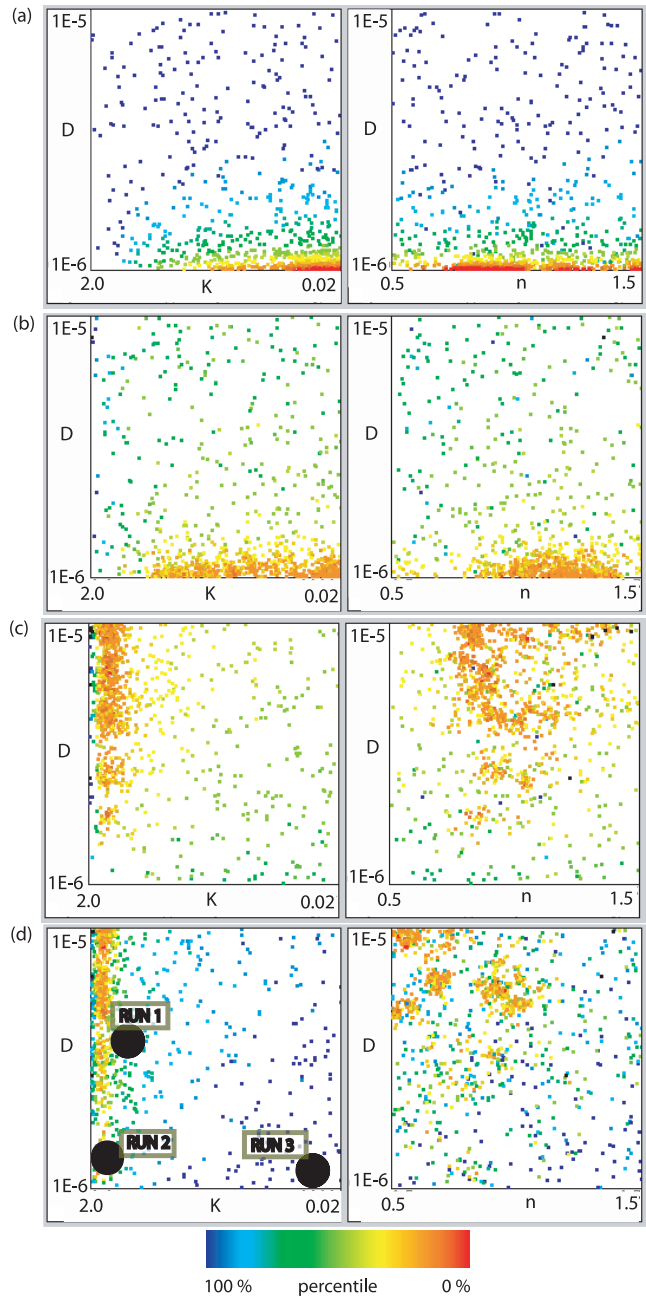

Figure 13. Results of neighborhood algorithm searches in parameter space defined by K (fluvial efficiency), D (diffusion parameter), and n (slope exponent). Forward models are run for (a) 1, (b) 10, (c) 50, and (d) 100 kyr.

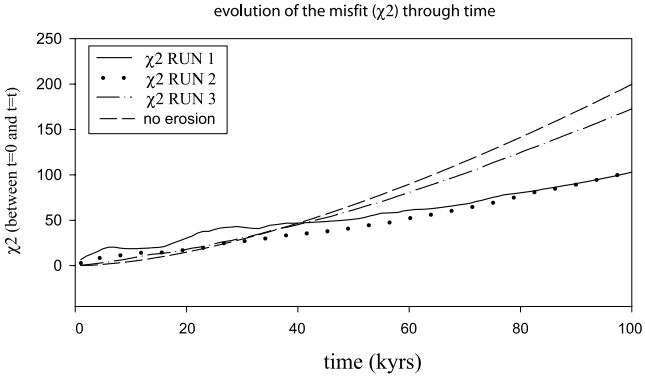

Figure 14. Evolution of the misfit value with time for RUN1, RUN2, and RUN3 and for the situation where no erosion takes place (tectonic signal).

the minimum calculated misfit function over the difference between minimum and maximum calculated misfits. Blue dots therefore represent forward models that lead to a maximized misfit whereas red ones correspond to a minimized misfit. As the NA proceeds, it concentrates in regions of the parameter space where the misfit function is minimized.

[50] The first two inversions (Figures 13a and 13b) show that over small time spans (1 and 10 kyr), there are no defined values of the river incision parameters K and n that can lead to topographic steady state. This means that the present-day topography is not at steady state and, potentially, can never be at steady state over such small timescales. Our interpretation is that even though valleys have V-shaped cross-sectional profiles and landform evolution appears to be dominated by fluvial processes, large parts of the landscape (i.e., near the divide) are still responding to the transition from glacial to fluvial conditions.

[51] For longer time runs (Figures 13c and 13d), the NA search converges to provide relatively strong constraints on the value of the fluvial erosion parameter K but not on the hillslope diffusion parameter D and the parameter n. We interpret this to mean that for longer time periods the only way to maintain a steady topography with our model is by substantial reshaping it through fluvial incision. This can also be interpreted to result from the different length scales at which the two processes operate. Over those timescales, diffusion is efficient at removing the details of the topography (i.e., at the hillslope size), whereas fluvial incision is capable of transforming the landscape over much greater distance. Because we define the misfit function at the scale of the landscape, it contains more information on long-range interactions between remote parts of the landscape than the evolution of individual hills.

[52] We illustrate this in Figure 14, where we plot the evolution with time of the misfit function for 3 different CASCADE runs represented in parameter space by the three large black circles (Figure 13d) with $m = 1/2$ and $n = 1$. RUN1 corresponds to high bedrock incision and high hillslope diffusion; RUN2 to high bedrock incision and low hillslope diffusion; RUN3 to low bedrock incision and low hillslope diffusion. For these three models, the misfit keeps increasing with time, indicating that no true geomorphic steady state can be achieved, principally due the tectonic horizontal advection of the landform. It is also instructive to compare the value of the misfit function for these three model runs to the misfit value obtained in a case where erosion is turned off. The "no-erosion" misfit value represents a measure of the change in landscape form due to tectonic uplift and horizontal advection. Early in their evolution, all model runs are characterized by a misfit value that is greater than the no-erosion run. Over long periods of time, all three models are characterized by lower misfit values than the no-erosion case. This confirms our previous assertion that the present-day topography is in a transient state.

[53] To highlight where relief modifications appear as the models progress, we display in Figures 15 and 16 the present-day topography on which we overlay the difference δh between the initial and final topographies at $t = 1$, 10, 50, and 100 kyr for two of the model runs (RUN1 and RUN2). The color contours are proportional to δh. The results from RUN1 and RUN2, for which bedrock incision is large, show that δh is positive in the bottom of valleys and negative on and near summits. This indicates that the best that the model can do when asked to keep the current landform at steady state leads to excessive uplift of the valley bottoms and erosion of the summits. This could obviously suggest that the stream power law adopted here is not a good representation of river incision. However, if the incision law is valid, this could be interpreted as indicating how the landscape evolves during the glacial-interglacial transition. Therefore it would indicate that the floors of most valleys have been "overflattened" by glacial erosion during the last glaciation or filled with glacial debris at the end of the glaciation, as previous field observations [*Adams*, 1980; *Whitehouse*, 1987], a recent seismic survey (T. Stern, personal communication, 2005) and topographic analyses (Figure 8) suggest, and have not yet recovered. In addition, the best fitting model predicts too much erosion at the top of the hills. This reshaping does not necessarily occur by hillslope diffusion (RUN1 and RUN2 are characterized by very different values of D but both show excess erosion on the peaks). It must therefore result from rapid incision along the tributary channels and subsequent landsliding. We interpret this result as another consequence of the strong glacial erosion of the main valleys that is keeping the base level of the tributaries anomalously low, therefore increasing their incision power. It could also be evidence that river tributaries have an important control on relief evolution, as previously suggested by *Whipple et al.* [1999].

[54] This interpretation is confirmed by a detailed examination of the evolution of the trunk channel relief, shown in Figure 17 for RUN1, RUN2 and RUN3. The lower reaches of the main trunk channel steepen with time while both the base level and the higher reaches remain at constant elevation. This may not be a true representation of reality since the downstream region is filled with postglacial and glacial outwash sediments. The main channel tends toward a steady state profile (Figure 17d) that is determined by a balance between erosion (itself proportional to slope and discharge) and tectonic uplift (which increases toward the Alpine Fault). The results presented in Figure 17 also show that topographic changes are small in the upstream part of the channels, where bedrock erosion is more efficient because of the higher slopes, and tectonic uplift is less

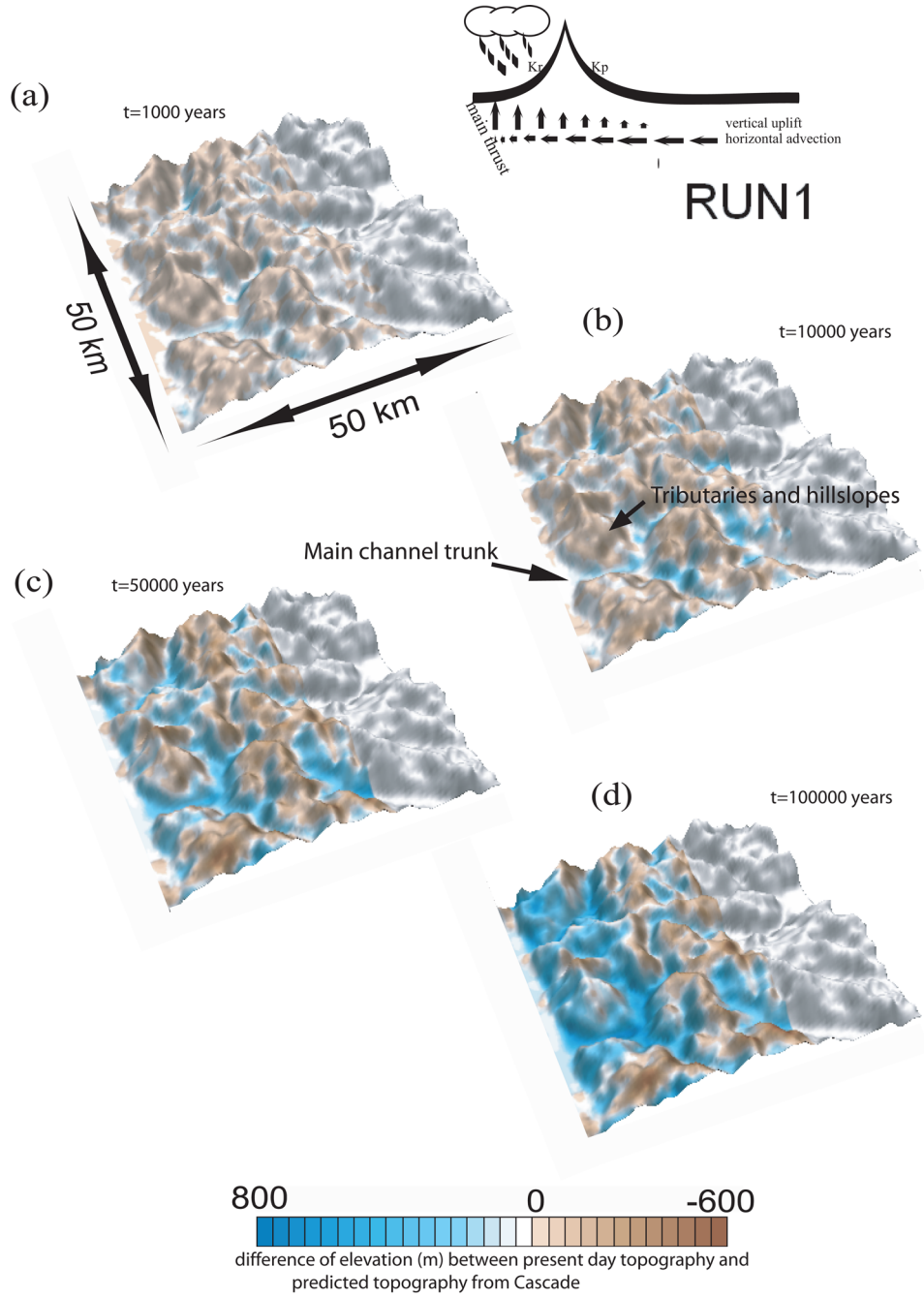

Figure 15. Present-day topography for model run RUN1 on which the difference between today's topography and topography at time t has been superimposed as color contours: (a) t = 1 kyr, (b) t = 10 kyr, (c) t = 50 kyr, and (d) t = 100 kyr.

important. Note that fluvial erosion near the divide would not be so efficient if we had introduced a significant threshold for bedrock incision as suggested by *Lague et al.* [2003].

6. Conclusions and Discussion

[55] The existing geomorphic and structural evidence points toward different mechanisms controlling the geomorphic evolution on either side of the Main Divide in the Southern Alps, New Zealand. On the western side, strong orographic precipitation combined with extreme rates of tectonic uplift are the processes that control the development and evolution of a mixed glacial-fluvial landscape. This landscape is episodically reshaped during and between glacial periods. On the eastern side, the geometry of large glacial valleys is initiated by differential uplift along large southwest-northeast trending faults that are antithetic to the Alpine Fault. We have confirmed these findings through a detailed analysis of the features of the landscape and by demonstrating that present-day seismicity, and thus fault activity, is confined to the eastern side of the orogen.

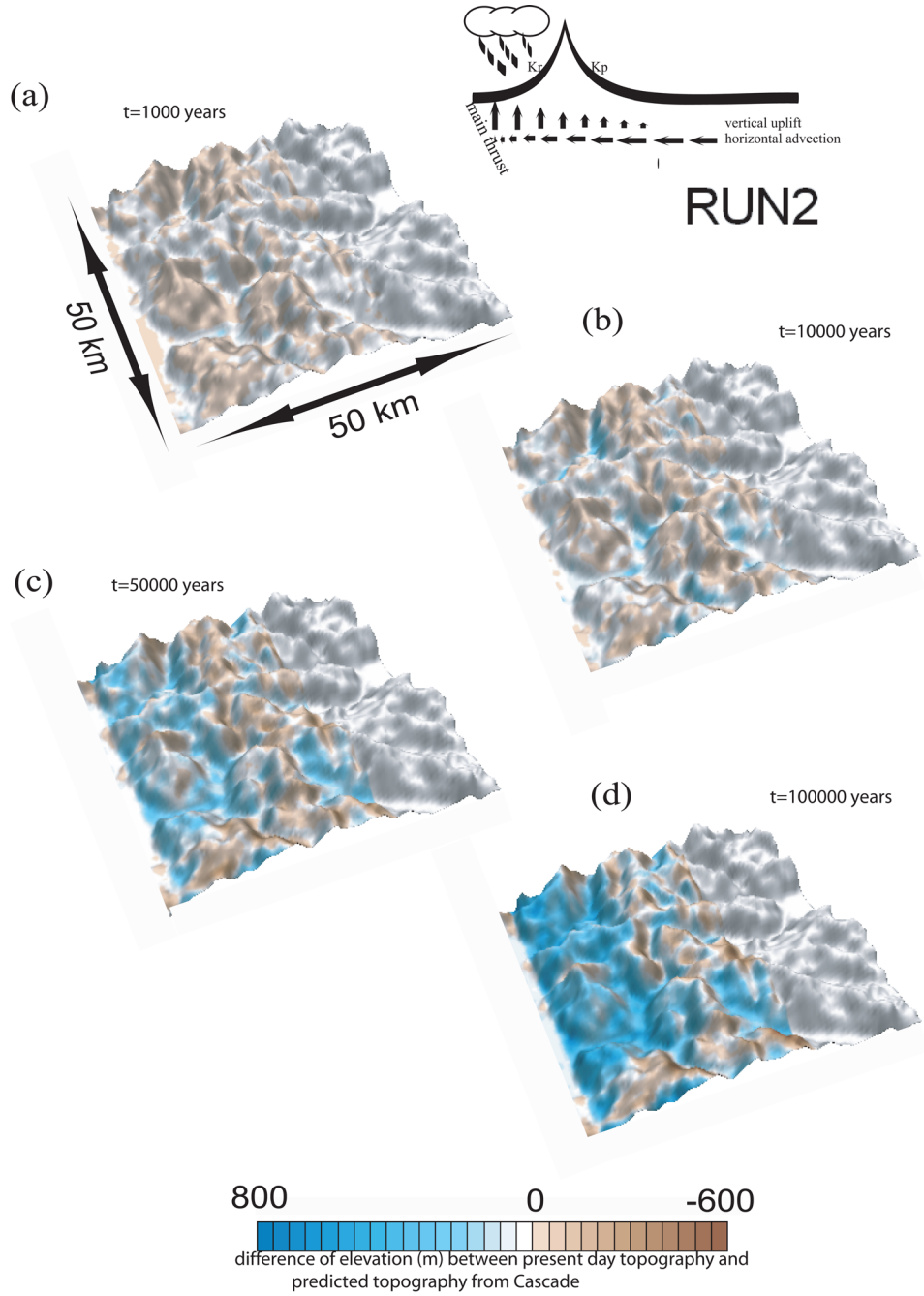

Figure 16. Same as Figure 15 but for model run RUN2.

[56] The results of a simple 1-D model of the evolution of the drainage divide show that the steady state position and height of the divide depends on the efficiency of fluvial incision and the difference in erosion between the prosides and retrosides of the orogen. The results of the numerical experiments also suggest that differences in tectonic velocity may lead to different positions of the divide (especially in the case when the divide is protected). This is exactly what is observed in the Southern Alps: going along the Alpine Fault from the northeast to the southwest, that is, from the mouth of the Harirari River to Fox Glacier (Figure 1a), the component of the relative velocity between the Australian and Pacific plates normal to the plate boundary decreases (Figure 1c) whereas the distance between the divide and the Alpine Fault increases (Figure 1b).

[57] In tectonically active mountain ranges strongly affected by glaciations, the transition from glacial to fluvial conditions perturbs the balance between erosion and tectonic uplift and can thus be regarded as a natural experiment to help us understand how either of these two landforming processes behaves on geological timescales. The results of our 2-D model shows that such a transition leads to a reduction of the ridge to bottom relief: the trunk is uplifted and the ridges levelled down. In the case of the Southern Alps, this reduction of relief will most likely never reach steady state conditions since warmer, interglacial periods

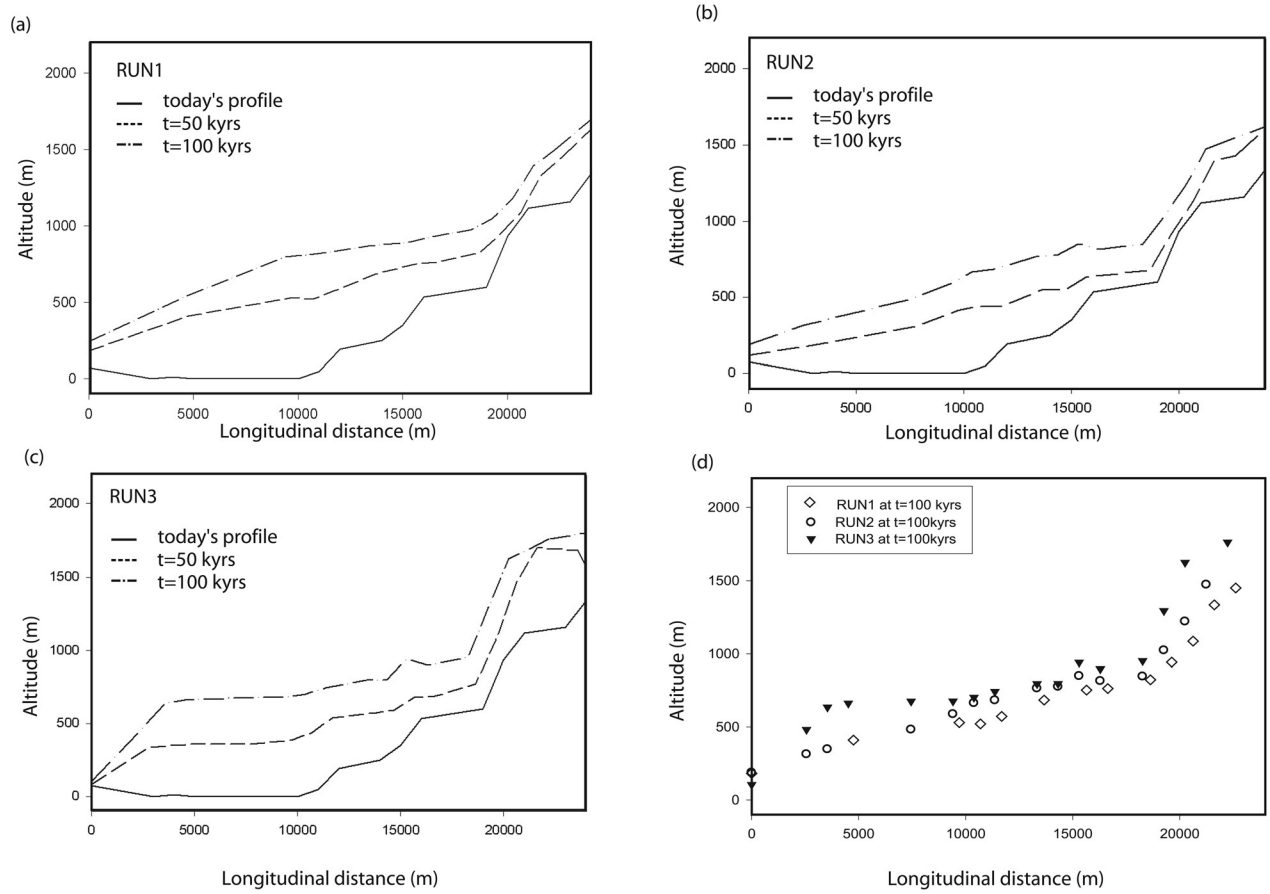

Figure 17. Evolution of the trunk channel altitude during numerical simulations: (a–c) evolution of the trunk during the experiment and (d) the trunk at the end of each experiment. Note that the steps in the initial profile are enhanced by the coarse resolution of the grid, and RUN3 corresponds to a scenario where nearly no erosion is applied.

are shorter than glacial periods and because of the high rate of lateral tectonic advection of the landscape toward its base level, the Alpine Fault. The numerical exercise also shows that landscape modifications are principally driven by river tributaries which, following transition to fluvial conditions, see a base level drop and, consequently, develop an enhanced potential for erosion.

[58] While the topographic divide tends to evolve toward a steady state position, the landform remains affected by the horizontal advection. Hence, in a framework of reference attached to the divide, the horizontal transport of the geomorphic features toward and through the drainage divide is inevitable. Evidence in the landscape of the Southern Alps suggests that transfers of the basins across the divide do occur, and potentially by discrete jumps [*Craw et al.*, 2004]. Such discrete transfers imply that some of the large-scale characteristics of the landform on the western side of the orogen, that is, the location and orientation of major valleys, are inherited from the evolution of the landscape on the other side. Our 1-D model predicts the equilibrium position of the divide, but does not address how features of the landscape may cross the divide. We postulate that transfers may happen during glacial periods, when the ice divide may not locally correspond to the topographic divide. These are also likely to take place during the transition between glacial and nonglacial periods, which must correspond to phases of change in the erosional regime and lead to substantial shifts in the equilibrium position and height of the divide. In an environment where the mean erosion rate varies between 1 and 10 km Myr^{-1}, the timescale over which these changes take place is certainly comparable to the period of the climate cycles.

[59] Moreover, the difference in the geometry of the drainage basins on either side of the divide seems to suggest that the landform can very rapidly adapt to the extreme change in environment. For instance, the Whataroa drainage basin appears to be in a transitional state. The Perth River and the upper reaches of the Whataroa River (Figures 3 and 6a) have long and deep segments that run parallel to the drainage divide and could be interpreted as remnant of a large glacial trough that developed along a ancient proshear. As this drainage basin was advected it may have passed across the Main Divide, where it became progressively dissected by a network of rivers, most likely tributaries, that run perpendicular to the divide in the direction of maximum slope. Our 2-D model suggests that these tributaries can be very efficient. Finally, when a catchment belonging to the eastern side of the drainage is eventually advected on the western side, the size of the drainage area on the western flank will increase proportionally. In turn, this will be equivalent to an

increase of erosion on the retroside of the orogen and induce a farther migration of the divide toward the southeast, as suggested by our 1-D model.

[60] To conclude, we have shown that landforms in the Southern Alps are the product of several processes: the strong asymmetry in tectonic uplift (potentially related to the orographically imposed asymmetry in rainfall), tectonic advection and the onset of cyclic glaciations some 2–3 Myr ago. We have attempted here to document and quantify the interactions between the various processes at play. We suggest, however, that a proper understanding of the complex interactions outlined here requires (1) the collection of low-temperature thermochronological data on the west side of the orogen, at all wavelengths of the topography and all elevations, to unravel the efficiency of each of the proposed mechanisms, (2) the collection of a thermochronological data set that would enable estimation of the amount of faulting and erosion on the southwest-northeast trending faults of the eastern side of the orogen, and (3) development of numerical models that allow for the coupled analysis of tectonic uplift and advection with fluvial and glacial erosion and the feedback from erosion to tectonics.

[61] **Acknowledgments.** Some of the computations presented here have been performed on the Terrawulf facility of the Centre for Advanced Data Inference at the Research School of Earth Sciences, Australian National University. The authors also thank the Australian Research Council for funding (ARC discovery grant DP0342909). The authors would like to thank Derek Fabel and Tim Barrows for stimulating discussions and Steven Micklethwaite for his help during the preparation of this manuscript, as well as Simon Brocklehurst, Andrew Meigs, the associate editor, and Robert Anderson for their thoughtful reviews on previous versions of this manuscript.

References

Adams, C. J. (1980), Contemporary uplift rates and erosion of the Southern Alps, New Zealand, *Geol. Soc. Am. Bull.*, *91*, 1–114.

Allis, R. G. (1981), Continental underthrusting beneath the Southern Alps of New Zealand, *Geology*, *9*, 303–307.

Allis, R. G. (1986), Mode of crustal shortening adjacent to the Alpine Fault, New Zealand, *Tectonics*, *5*(1), 15–32.

Avouac, J.-P., and E. Burov (1996), Erosion as a driving mechanism of intracontinental mountain growth, *J. Geophys. Res.*, *101*, 17,747–17,769.

Barrows, T. T., S. Juggins, P. De Deckker, J. Thiede, and J. Martinez (2000), Sea-surface temperatures of the southwest Pacific Ocean during the Last Glacial Maximum, *Paleoceanography*, *15*, 95–109.

Batt, G. E. (1997), The crustal dynamics and tectonic evolution of the Southern Alps, New Zealand: Insights from new geochronological data and fully-coupled thermo-dynamical finite element modeling, Ph.D. thesis, Aust. Natl. Univ., Canberra.

Batt, G. E., and J. Braun (1997), On the thermomechanical evolution of compressional orogens, *Geophys. J. Int.*, *128*, 364–382.

Batt, G. E., and J. Braun (1999), The tectonic evolution of the Southern Alps, New Zealand: Insights from fully thermally coupled dynamical modelling, *Geophys. J. Int.*, *136*, 403–420.

Batt, G. E., J. Braun, B. P. Kohn, and I. McDougall (2000), Thermochronological analysis of the dynamics of the Southern Alps, New Zealand, *Geol. Soc. Am. Bull.*, *112*, 250–266.

Beaumont, C., P. Fullsack, and J. Hamilton (1992), Erosional control of active compressional orogens, in *Thrust Tectonics*, edited by K. R. McClay, pp. 1–18, CRC Press, Boca Raton, Fla.

Beaumont, C., P. Fullsack, and J. Hamilton (1994), Styles of crustal deformation in compressional orogens caused by subduction of the underlying lithosphere, *Tectonophysics*, *232*, 119–132.

Beaumont, C., S. Ellis, J. Hamilton, and P. Fullsack (1996a), Mechanical models for subduction-collision tectonics of Alpine-type compressional orogens, *Geology*, *24*, 675–678.

Beaumont, C., P. J. J. Kamp, J. Hamilton, and P. Fullsack (1996b), The continental collision zone, South Island, New Zealand: Comparison of geodynamical models and observations, *J. Geophys. Res.*, *101*, 3333–3359.

Beaumont, C., R. A. Jamieson, M. H. Nguyen, and B. Lee (2001), Himalayan tectonics explained by extrusion of a low-viscosity crustal channel coupled to focused surface denudation, *Nature*, *414*, 738–742.

Beaumont, C., R. A. Jamieson, M. H. Nguyen, and S. Medvedev (2004), Crustal channel flows: 1. Numerical models with applications to the tectonics of the Himalayan-Tibetan orogen, *J. Geophys. Res.*, *109*(0), B06406, doi:10.1029/2003JB002809.

Beavan, J., et al. (1999), Crustal deformation during 1994–1998 due to oblique continental collison in the central Southern Alps, New Zealand, and implications for seismic potential of the Alpine Fault, *J. Geophys. Res.*, *104*, 25,233–25,255.

Beavan, R., P. Tregoning, M. Bevis, T. Kato, and M. C. Meertens (2002), Motion and rigidity of the Pacific plate and implications for plate boundary deformation, *J. Geophys. Res.*, *107*(B10), 2261, doi:10.1029/2001JB000282.

Braun, J., and C. Beaumont (1995), Three-dimensional numerical experiments of strain partitioning at oblique plate boundaries: Implications for contrasting tectonic styles in the southern Coast Ranges, California and central South Island, New Zealand, *J. Geophys. Res.*, *100*, 18,059–18,074.

Braun, J., and M. Sambridge (1997), Modelling landscape evolution on geological time scales: A new method based on irregular spatial discretization, *Basin Res.*, *9*, 27–52.

Braun, J., G. E. Batt, D. L. Scott, H. McQueen, and A. R. Beasley (1994), A simple kinematic model for crustal deformation along two- and three-dimensional listric normal faults derived from scaled laboratory experiments, *J. Struct. Geol.*, *16*, 1477–1490.

Braun, J., A. Heimsath, and J. Chapell (2001), Sediment transport mechanisms on soil-mantled hillsploes, *Geology*, *29*, 683–686.

Brocklehurst, S. H. (2003), Evolution of topography in glaciated mountain ranges, Ph.D. thesis, Mass. Inst. of Technol., Cambridge.

Brocklehurst, S. H., and K. X. Whipple (2002), Glacial erosion and relief production in the eastern Sierra Nevada, *Geomorphology*, *42*, 1–24.

Brozovic, N., D. W. Burbank, and A. J. Meigs (1997), Climatic limits on landscape development in the northwestern Himalayas, *Science*, *276*, 571–574.

Brune, J. N. (1968), Seismic moment, seismicity, and rate of slip along major fault zones, *J. Geophys. Res.*, *72*, 777–784.

Chase, C. G. (1992), Fluvial landscuplting and the fractal dimension of topography, *Geomorphology*, *5*, 39–57.

Cox, S., and R. H. Findley (1995), The Main Divide fault zone and its role in the formation of the Southern Alps, *N. Z. J. Geol. Geophys.*, *38*, 489–500.

Craw, D., M. S. Rattenbury, and R. D. Johnstone (1994), Structures within greenschist facies alpine schist, central Southern Alps, *N. Z. J. Geol. Geophys.*, *37*, 101–111.

Craw, D., E. Nelson, and P. Koons (2004), Structure and topographic evolution of the Main Divide in the Landsborough-Hopkins area of the Southern Alps, New Zealand, *N. Z. J. Geol. Geophys.*, *46*, 553–562.

Davey, F. J., T. Henyey, S. Kleffman, A. Melhuish, D. Okaya, and T. Stern (1995), Crustal reflections from the Alpine Fault zone, South Island, New Zealand, *N. Z. J. Geol. Geophys.*, *38*, 601–604.

Davis, D., J. Suppe, and F. A. Dahlen (1983), Mechanics of fold-and-thrust belts and accretionary wedges, *J. Geophys. Res.*, *88*, 1153–1172.

Davis, W. M. (1892), The convex profile of badland divides, *Science*, *20*, 245.

Densmore, A. L., M. E. Ellis, and R. S. Anderson (1998), Landsliding and the evolution of normal-fault-bounded mountains, *J. Geophys. Res.*, *103*, 15,203–15,219.

Finlayson, B. A. (1992), *Numerical Methods for Problems with Moving Fronts*, 1st ed., Ravenna Park, Seattle, Wash.

Gesto, F. (2003), Seismic strain, lithospheric deformation and surface topography, honours thesis, Aust. Natl. Univ., Canberra.

Gilbert, G. K. (1909), The convexity of hilltops, *J. Geol.*, *17*, 344–350.

Griffiths, G. A., and M. J. McSaveney (1983), Distribution of mean annual precipitation across some steepland regions of New Zealand, *N. Z. J. Sci.*, *26*, 197–209.

Gutenberg, B., and C. F. Richter (1944), Frequency of earthquakes in California, *Bull. Seismol. Soc. Am.*, *34*, 185–188.

Herman, F., and J. Braun (2006), A parametric study of soil transport mechanisms, in *Tectonics, Climate, and Landscape Evolution*, edited by S. Willett et al., *Geol. Soc. Am. Spec. Pap.*, *398*, 191–200.

Hovius, N., C. P. Stark, and P. A. Allen (1997), Sediment flux from a mountain belt derived from landslide mapping, *Geology*, *25*, 231–234.

Hovius, N., C. Stark, H. Chu, and J. Lin (2000), Supply and removal of sediment in a landslide-dominated mountain belt: Central Range, Taiwan, *J. Geology.*, *108*, 73–89.

Howard, A. D. (1994), A detachment-limited model of drainage basin evolution, *Water Resour. Res.*, *30*, 2261–2285.

Kamp, P., and J. Tippett (1993), Dynamic of Pacific plate crust in the South Island (New Zealand) zone of oblique continent-continent convergence, *J. Geophys. Res.*, *98*, 16,105–16,118.
Kirkbride, M., and D. Matthews (1997), The role of fluvial and glacial erosion in landscape evolution: Ben Ohau range, New Zealand, *Earth Surf. Processes Landforms*, *22*, 317–327.
Koons, P. O. (1987), Thermal and mechanical consequences of rapid uplift in continental collision: An example from the Southern Alps, New Zealand, *Am. J. Sci.*, *289*, 1041–1069.
Koons, P. O. (1994), Three-dimensional critical wedges: Tectonics and topography in oblique collision orogen, *J. Geophys. Res.*, *99*, 13,301–13,315.
Koons, P., R. Norris, D. Craw, and A. Cooper (2002), Influence of exhumation on the structural evolution of transpressional plate boundaries: An example from the Southern Alps, New Zealand, *Geology*, *31*, 3–6.
Kostrov, V. V. (1974), Seismic moment and energy earthquakes, and seismic flow of rocks, *Earth Phys.*, *1*, 23–40.
Lague, D., A. Crave, and P. Davy (2003), Laboratory experiments simulating the geomorphic response to tectonic uplift, *J. Geophys. Res.*, *108*(B1), 2008, doi:10.1029/2002JB001785.
Little, T. A., and R. J. Holcombe (2002), Kinematics of oblique collision and ramping inferred from microstructures and strain in middle crustal rocks, central Southern Alps, New Zealand, *J. Struct. Geol.*, *24*, 219–239.
MacGregor, K., R. S. Anderson, S. Anderson, and E. Waddington (2000), Numerical simulations of glacial longitudinal profile evolution, *Geology*, *28*, 1031–1034.
Molnar, P., and P. England (1990), Late Cenozoic uplift of mountain ranges and global climate change: Chicken and egg?, *Nature*, *346*, 29–34.
Molnar, P., and P. Taponnier (1975), Cenozoic tectonics of Asia: Effects of a continental collision, *Science*, *189*, 419–426.
Norris, R. J., and A. F. Cooper (2000), Late Quaternary slip rates and slip partitioning on the Alpine Fault, New Zealand, *J. Struct. Geol.*, *23*, 507–520.
Norris, R. J., P. O. Koons, and A. F. Cooper (1990), The obliquely convergent plates in the South Island of New Zealand: Implications for ancient collison zones, *J. Struct. Geol.*, *12*, 715–725.
Porter, S. C. (1975), Equilibrium-line altitudes of the late Quaternary glaciers in the Southern Alps, New Zealand, *Quat. Res.*, *5*, 27–47.
Pratt-Sitaula, B., D. W. Burbank, A. Heimsath, and O. Tank (2004), Landscape disequilibrium on 1,000–10,000 year scales, Marsayandi River, Nepal, central Himalaya, *Geomorphology*, *58*, 223–241.
Raymo, M. E., and W. F. Ruddiman (1992), Tectonic forcing of the late Cenozoic climate, *Nature*, *359*, 117–122.
Reiners, P. W., T. A. Ehlers, S. G. Mitchell, and D. R. Montgomery (2003), Coupled spatial variations in precipitation and long-term erosion rates across the Washington Cascades, *Nature*, *426*, 645–647.
Roering, J. J., L. S. Kirchner, J. Sklar, and W. E. Dietrich (2000), Hillslope evolution by nonlinear creep and landsliding: An experimental study, *Geology*, *29*, 143–146.
Sambridge, M. (1999a), Geophysical inversion with a neighbourhood algorithm: I. Searching a parameter space, *Geophys. J. Int.*, *138*, 479–494.
Sambridge, M. (1999b), Geophysical inversion with a neighbourhood algorithm: II. Appraising the ensemble, *Geophys. J. Int.*, *138*, 727–746.
Schlunegger, F., and M. Hinderer (2001), Crustal uplift in the Alps: Why the drainage pattern matters, *Terra Nova*, *13*(6), 425–432.
Schmidt, K. M., and D. R. Montgomery (1995), Limits to relief, *Science*, *270*, 617–620.
Small, E. E., and R. S. Anderson (1998), Pleistocene relief production in Laramide mountain ranges, western United States, *Geology*, *26*, 123–126.
Soons, J. M. (1979), Late Quaternary environments in the central South Island of New Zealand, *N. Z. Geogr.*, *35*, 16–23.
Stern, T. A. (1995), Gravity anomalies and crustal loading at and adjacent to the Alpine Fault, New Zealand, *N. Z. J. Geol. Geophys.*, *38*, 593–600.
Suggate, R. P. (1990), Late Pliocene and Quaternary glaciations of New Zealand, *Quat. Sci. Rev.*, *9*, 175–197.
Tomkin, J. (2000), Landforming processes in glaciated orogens: A numerical study, Ph.D. thesis, Aust. Natl. Univ., Canberra.
Walcott, R. I. (1998), Present tectonics and late Cenozoic evolution of New Zealand, *Rev. Geophys.*, *36*, 1–26.
Wellman, H. (1979), An uplift map for the South Island of New Zealand, and a model for uplift of the Southern Alps, in *The Origin of the Southern Alps*, edited by R. I. Walcott and M. M. Cresswell, pp. 13–20, R. Soc. of N. Z., Wellington, New Zealand.
Whipple, K. X., and G. E. Tucker (1999), Dynamics of the stream-power river incision model: Implications for height limits of mountain ranges, landscape response timescales, and research needs, *J. Geophys. Res.*, *104*, 17,661–17,674.
Whipple, K. X., E. Kirby, and S. H. Brocklehurst (1999), Geomorphic limits to climate-induced increases in topographic relief, *Nature*, *401*, 39–43.
Whitehouse, I. E. (1987), Geomorphology of a compressional plate boundary: Southern Alps, New Zealand, in *International Geomorphology, 1986: Proceedings of the First International Conference on Geomorphology*, part 1, edited by V. Gardiner, pp. 897–924, John Wiley, Hoboken, N. J.
Willett, R. W. (1950), The New Zealand Pleistocene snowline, climatic conditions and suggested biological effect, *N. Z. J. Sci. Technol., Sect. B*, *32*, 18–48.
Willett, S. D. (1999), Orogeny and orography: The effects of erosion on the structure of mountain belts, *J. Geophys. Res.*, *104*, 28,957–28,981.
Willett, S. D., and M. Brandon (2002), On steady state in mountains belts, *Geology*, *30*, 175–178.
Willett, S., C. Beaumont, and P. Fullsack (1993), Mechanical model for the tectonics of doubly-vergent compressional orogens, *Geology*, *21*, 371–374.
Willett, S. D., R. Slingerland, and N. Hovius (2001), Uplift, shortening, and steady state topography in active mountain belts, *Am. J. Sci.*, *301*, 455–485.
Wobus, C. W., K. V. Hodges, and K. X. Whipple (2003), Has focused denudation sustained active thrusting at the Himalayan topographic front?, *Geology*, *31*, 861–864.
Zeitler, P. K., et al. (2001), Crustal reworking at Nanga Parbat, Pakistan: Evidence for erosional focusing of crustal strain, *GSA Today*, *11*, 4–8.

J. Braun, Géosciences Rennes, Université de Rennes 1, Campus de Beaulieu CS 74205, F-35042 Rennes Cedex, France.
F. Herman, California Institute of Technology, Pasadena, CA 91125, USA. (frederic@gps.caltech.edu)